Epithelial junction formation requires confinement of Cdc42 activity by a novel SH3BP1 complex

Ahmed Elbediwy,[1] Ceniz Zihni,[1] Stephen J. Terry,[1] Peter Clark,[2] Karl Matter,[1] and Maria S. Balda[1]

[1]Department of Cell Biology, Institute of Ophthalmology, University College London, EC1V 9EL London, England, UK
[2]National Heart and Lung Institute, Imperial College London, South Kensington Campus, SW7 2AZ London, England, UK

Epithelial cell–cell adhesion and morphogenesis require dynamic control of actin-driven membrane remodeling. The Rho guanosine triphosphatase (GTPase) Cdc42 regulates sequential molecular processes during cell–cell junction formation; hence, mechanisms must exist that inactivate Cdc42 in a temporally and spatially controlled manner. In this paper, we identify SH3BP1, a GTPase-activating protein for Cdc42 and Rac, as a regulator of junction assembly and epithelial morphogenesis using a functional small interfering ribonucleic acid screen. Depletion of SH3BP1 resulted in loss of spatial control of Cdc42 activity, stalled membrane remodeling, and enhanced growth of filopodia. SH3BP1 formed a complex with JACOP/paracingulin, a junctional adaptor, and CD2AP, a scaffolding protein; both were required for normal Cdc42 signaling and junction formation. The filamentous actin–capping protein CapZ also associated with the SH3BP1 complex and was required for control of actin remodeling. Epithelial junction formation and morphogenesis thus require a dual activity complex, containing SH3BP1 and CapZ, that is recruited to sites of active membrane remodeling to guide Cdc42 signaling and cytoskeletal dynamics.

Introduction

Epithelial junction assembly and morphogenesis are driven by a complex set of cytoskeletal rearrangements that drive dynamic membrane remodeling and the necessary cell shape changes that underlie the formation of functional epithelial tissues (Nelson, 2009). Although there are variations among different epithelia, junction formation is generally induced by filopodia or lamellipodia initiating cell–cell contact followed by junction formation and maturation, leading to the establishment of mature tight and adherens junctions (Vasioukhin et al., 2000; Matter and Balda, 2003b; Miyoshi and Takai, 2008; Nelson, 2009). Actin remodeling underlies these morphological transitions and needs to be carefully controlled to allow the coordinated assembly of a functional apical junctional complex (Vasioukhin et al., 2000; Redd et al., 2004; Chhabra and Higgs, 2007).

RhoGTPases are central regulatory switches that guide actin organization, junction formation, and epithelial differentiation (Braga and Yap, 2005; Jaffe and Hall, 2005; Ridley, 2006). They are regulated by factors that catalyze the switch between the active, GTP-bound state, and the inactive, GDP-bound state: activation is mediated by guanine nucleotide exchange factors (GEFs) and inactivation by GTPase-activating proteins (GAPs; Bos et al., 2007). The RhoGTPase Cdc42 is an evolutionarily conserved regulator of cell polarization and regulates different steps of junction formation from filopodial extension to junctional maturation; hence, mechanisms must exist that activate and inactivate Cdc42 in a temporally controlled manner at specific subcellular sites to permit progression of dynamic morphological processes (Matter and Balda, 2003b; Iden and Collard, 2008). Although activation of Cdc42 is generally seen as the critical step, expression of dominant-negative and constitutively active mutants of Cdc42 revealed that inhibition as well as overstimulation of Cdc42 signaling prevents normal junction formation and differentiation (Kroschewski et al., 1999; Rojas et al., 2001; Bruewer et al., 2004). Hence, negative regulation of Cdc42 is important for the successful completion of complex sequential Cdc42-driven processes. This is supported by

K. Matter and M.S. Balda contributed equally to this paper.

Correspondence to Karl Matter: k.matter@ucl.ac.uk; or Maria S. Balda: m.balda@ucl.ac.uk

S.J. Terry's present address is Randall Division of Cell and Molecular Biophysics, King's College London, WC2R 2LS London, England, UK.

Abbreviations used in this paper: Erk, extracellular signal–regulated kinase; FRET, fluoresecence/Förster resonance energy transfer; GAP, GTPase-activating protein; GEF, guanine nucleotide exchange factor; HCE, human corneal epithelial.

The Rockefeller University Press $30.00
J. Cell Biol. Vol. 198 No. 4 677–693
www.jcb.org/cgi/doi/10.1083/jcb.201202094

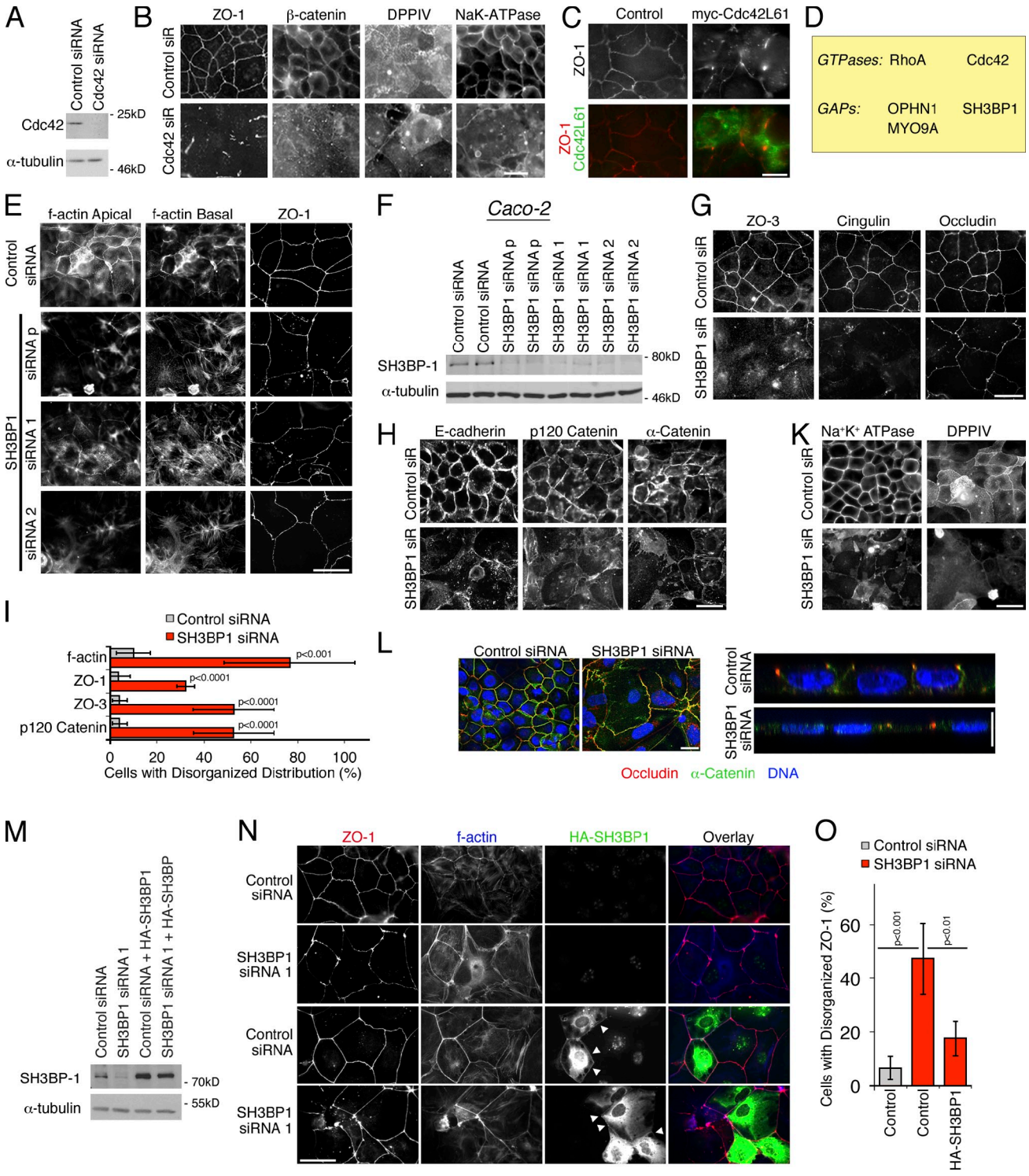

Figure 1. **SH3BP1 depletion disrupts epithelial cell–cell junctions.** (A and B) Caco-2 cells were transfected with control and Cdc42-directed siRNAs (50 nM) and then analyzed by immunoblotting (A) and immunofluorescence (B). Shown are epifluorescence images. (C) Caco-2 cells were transfected with myc-tagged Cdc42L61, a constitutively active mutant, and then stained for ZO-1 and the transfected protein. (D) Summary of RhoGTPases and GAPs identified in the functional siRNA screen (see also Table S1). (E–L) Caco-2 cells were transfected with siRNAs as indicated and then analyzed by immunofluorescence (E and G–L) or immunoblotting (F). Apart from F-actin, shown are images of markers for tight junctions (E and G), adherens junctions (H), and basolateral and apical cell surface domains (K). Shown are epifluorescence (D and F–K) and confocal (L, xy and z sections are provided) images. For F-actin, apical and basal focal planes are shown. Panel I shows a quantification of the effect on the subcellular distribution of F-actin (counting cells with strongly induced basal F-actin; mean basal actin intensity increased by >60% in SH3BP1-depleted cells) and three junctional markers (counting cells with discontinuous, irregular junctional staining). Shown are means ± 1 SD, representing the cells in at least five different fields per condition ($n \geq 5$). Note that assembly of tight and adherens junctions is affected, but different components are affected to different extents. (M–O) Complementation of SH3BP1 siRNA transfection with a siRNA-resistant cDNA. Caco-2 cells were first transfected with siRNAs as indicated and then, after 3 d, with a plasmid carrying the siRNA-resistant cDNA. Cells were then analyzed by immunoblotting (M) or immunofluorescence (N). Panel O shows a quantification of the ZO-1 staining (six fields for each condition). The arrowheads in N point to staining for myc-SH3BP1 along cell–cell contacts. Error bars show SDs. Bars, 10 µm. p, phosphorylated.

the finding that Rich1, a GAP for Cdc42, is required for full polarization of epithelial cells (Wells et al., 2006). However, Rich1 is thought to regulate polarization once junctions are assembled, as it is not required for membrane dynamics and adherens junction assembly. Whether specific GAPs are required for junction assembly and are important to maintain actin dynamics and membrane remodeling is not known. Moreover, it is likely that GTPase regulation is tightly connected to other regulators of actin dynamics; however, little is known about specific molecular cross talk that would mediate such cooperative regulatory mechanisms.

Here, we use a functional siRNA screen to identify GAPs important for epithelial morphogenesis that led to the identification of SH3BP1 as a crucial regulator of epithelial junction formation and morphogenesis. SH3BP1 is a GAP for Rac and Cdc42 (Cicchetti et al., 1995; Parrini et al., 2011), and our data show that its depletion leads to spatial and temporal deregulation of Cdc42 and, depending on the cell model, a modest effect on Rac activation. SH3BP1 forms a complex with two scaffolding proteins and the F-actin–capping protein CapZ, suggesting that this regulatory complex represents a dual activity module that links regulation of Cdc42 and actin dynamics during membrane remodeling and junction formation.

Results

SH3BP1 is required for epithelial junction formation and morphogenesis

We used the intestinal epithelial cell line Caco-2 as a model system to screen for functionally relevant Rho GAPs, as these cells form polarized monolayers and can be efficiently transfected with siRNAs (Terry et al., 2011). The siRNA-mediated depletion of Cdc42 was efficient and led to flatter cells with a disrupted distribution of ZO-1, a tight junction protein, and β-catenin, a component of adherens junctions as well as reduced and disorganized expression of the apical marker DPPIV and the basolateral protein Na^+K^+-ATPase (Fig. 1, A and B). Similarly, overexpression of constitutively active Cdc42, myc-Cdc42L61, disrupted the normal organization of cell junctions and the actin cytoskeleton in Caco-2 as well as in the epidermal carcinoma cell line A431 (Fig. 1 C and Fig. S1 A). Hence, inhibition as well as overstimulation of Cdc42 interferes with normal epithelial junction formation and differentiation as previously observed in other epithelial cell systems (Kroschewski et al., 1999; Rojas et al., 2001; Bruewer et al., 2004).

We next combined this morphological assay for junction assembly and polarization with an siRNA library targeting RhoGTPases and GAPs to identify RhoGTPase regulators important for junction formation. Potential candidates identified in the first round of screening using standard siRNAs were retested in a second round using siRNAs modified to enhance specificity (Tables S1, S2, and S3).

Depletion of the two RhoGTPases RhoA and Cdc42 led to clearly the strongest phenotypes followed by the Cdc42 GAP SH3BP1 and two RhoA GAPs, OPHN1 and MYO9A (Fig. 1 D and Fig. S1 B). Regulation of RhoA is crucial during epithelial junction formation (Terry et al., 2011), and both identified RhoA GAPs MYO9A (Abouhamed et al., 2009; Omelchenko and Hall, 2012) and OPHN1 (Fig. S1, C–E) localize to the junctional complex. OPHN1 has also GAP activity for Rac and Cdc42 in vitro; however, its main function in vivo seems to be regulation of RhoA (Billuart et al., 1998; Khelfaoui et al., 2009).

Depletion of SH3BP1 caused the strongest phenotype of all GAPs tested. Subsequent analysis in Caco-2 cells using different siRNAs resulted in monolayers that failed to assemble a normal junctional actin belt and exhibited a strong induction of basal F-actin, often in an astral shape along cell borders (Fig. 1, E and F). Similar patterns of disorganized actin were observed when cells were stained with β-actin antibodies instead of phalloidin (Fig. S2 A). Tight and adherens junctions were also affected, as markers such as ZO-1, cingulin, E-cadherin, and p120 catenin exhibited enhanced cytoplasmic staining and were less concentrated along cell–cell contacts (Fig. 1, G–I). Cells also failed to differentiate normally, as the distributions of DPPIV and Na^+K^+-ATPase were disrupted, although expression levels were not affected (Fig. 1 K and Fig. S2 B). Depleted cells remained flat and did not form columnar cells with distinct tight and adherens junctions and, hence, were less densely packed (Fig. 1 L). Similarly, in SH3BP1-depleted human corneal epithelial (HCE) cells, a squamous epithelial cell type, ZO-1, did not form a continuous junctional belt, and the adherens junction marker β-catenin accumulated in filopodia-like structures (Fig. S2 C). In the epidermal carcinoma cell line A431, depletion also triggered a reorganization of F-actin, resulting in accumulation of filopodia (Fig. S2 D). SH3BP1 is thus required for normal junction formation in epithelial cell models originating from different tissues and representing different types of epithelia. The accumulation of filopodia suggests that depletion may lead to deregulation of Cdc42.

We next introduced silent mutations into an SH3BP1 cDNA to generate an siRNA-resistant construct. Immunoblotting demonstrated that the construct was efficiently expressed in cells transfected with control and SH3BP1-specific siRNAs (Fig. 1 M). Immunofluorescence revealed that the siRNA-resistant construct indeed counteracted the depletion-induced phenotype (Fig. 1, N and O). Ectopically expressed SH3BP1 was enriched at cell–cell junctions, suggesting that the GAP may interact with junctional components. However, the overexpressed protein also accumulated in the cytosol, suggesting that its targeting is easily saturated or may be a dynamically regulated.

We next asked whether Caco-2 cells were still able to form functional tight junctions upon depletion of SH3BP1. To monitor de novo junction formation, we performed Ca switch assays, in which cells are plated in low calcium and junction formation is then induced in a synchronized manner by the addition of calcium. Cells spread out normally after calcium addition, but conversion to a continuous peripheral actin belt did not occur, and junctional markers were not recruited efficiently (Fig. 2, A–D; and Fig. S2, E and F). Consequently, the barrier properties of SH3BP1-depleted cells were strongly compromised (Fig. 2, E and F).

During de novo junction formation in keratinocytes, filopodia initiate cell–cell contacts followed by formation of a zipperlike

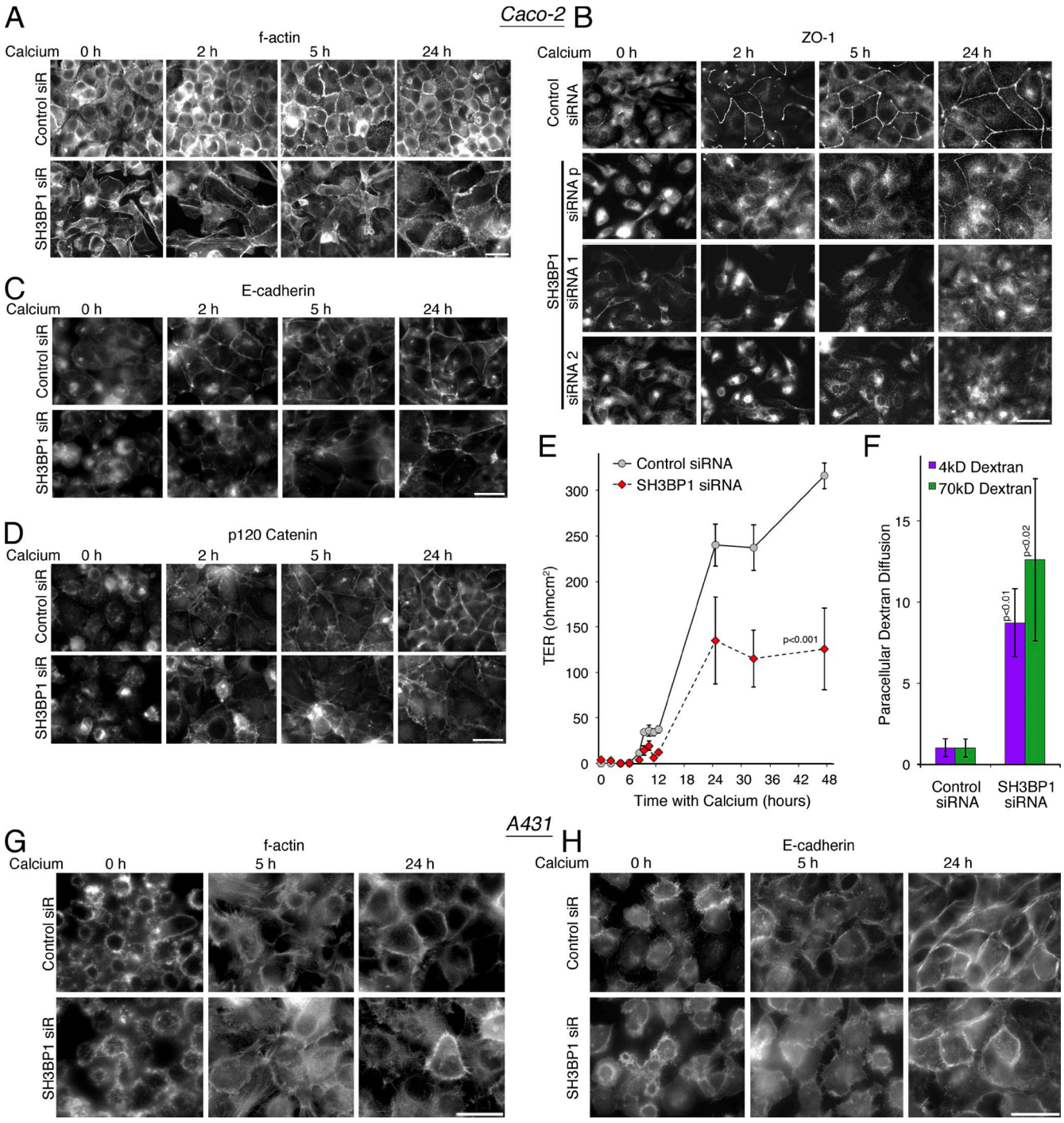

Figure 2. **SH3BP1 regulates epithelial junction formation.** (A–F) Caco-2 cells transfected with siRNAs were plated in low calcium medium before adding calcium to induce junction formation, which was followed by staining with fluorescent phalloidin (A), ZO-1 (B), E-cadherin (C), p120 catenin (D), or by measuring transepithelial electrical resistance (TER; E). (F) After 48 h, paracellular tracer diffusion was measured. E and F show means ± 1 SD; $n = 3$. (G and H) siRNA-transfected A431 cells were plated in low calcium medium and then stimulated for different periods of time with calcium to induce junction formation. Shown are images of cells stained phalloidin (G) or with anti–E-cadherin antibodies (H). Note that depletion of SH3BP1 leads to a strong induction of E-cadherin–positive filopodia. Bars, 10 µm. p, phosphorylated.

belt that precedes formation of mature junctions (Vasioukhin et al., 2000). Therefore, the accumulation of filopodia in SH3BP1-depleted A431 may reflect a failure in the transition from filopodia to cell junctions. Addition of calcium to A431 cells plated in low calcium resulted in the induction of filopodia-based cell–cell contacts, enriched in F-actin and E-cadherin, followed by formation of continuous adherens junctions over the course of a few hours (Fig. 2, G and H). In contrast, SH3BP1-depleted cells formed contacts, but they did not progress beyond the stage of forming intercalating filopodia, indicating that SH3BP1 is required for the transition from early cell–cell contacts to cell junctions.

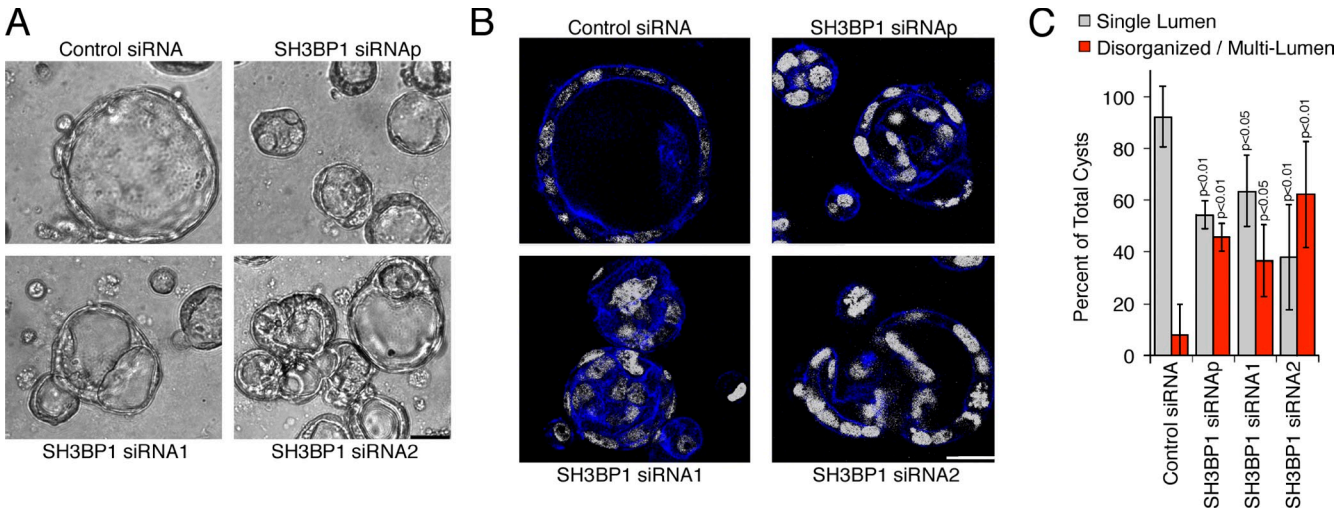

Figure 3. **SH3BP1 regulates epithelial morphogenesis.** (A–C) Caco-2 cells were transfected with siRNAs and then plated in a 3D matrix. After 5 d, the cells were fixed and first analyzed by phase-contrast microscopy (A) before staining with fluorescent phalloidin and Hoechst followed by confocal microscopy (B). Note that SH3BP1 depletion leads to smaller and often disorganized cysts. The effect of SH3BP1 depletion was quantified by counting normally organized cysts with a single lumen and disorganized cysts with no or multiple lumen (only cysts that had reached a minimal size of 30-µm diameter were considered for the morphological quantification to avoid a bias because of the smaller cysts). Shown are means ± 1 SD of three independent experiments (n = 3). Bars, 10 µm. p, phosphorylated.

We next determined whether SH3BP1 is also important for epithelial morphogenesis in an organotypic 3D culture system. Fig. 3 A shows that depletion of the GAP resulted in generally smaller and poorly organized cysts. Actin staining demonstrated that SH3BP1 depletion led to cysts that often formed multiple instead of a single lumen (Fig. 3 B). Quantification of these experiments indeed supported the conclusion that SH3BP1 is essential for epithelial morphogenesis in a 3D culture system (Fig. 3 C). These experiments thus indicate that SH3BP1 is a critical regulator of junction formation and epithelial morphogenesis in cell models derived from different epithelial tissues.

SH3BP1 colocalizes with the junctional complex

As overexpressed SH3BP1 was recruited to cell junctions (Fig. 1 N), we tested whether endogenous SH3BP1 also associates with cell junctions. Fig. 4 A shows that staining for SH3BP1 was indeed enriched at the junctional complex. Junctional SH3BP1 overlapped with β-catenin and occludin. There was also staining in the nucleus and the cytosol; however, only the junctional staining completely disappeared when SH3BP1 was depleted, suggesting that the nonjunctional staining might be partly nonspecific (Fig. 4 B). Confocal microscopy further supported the junctional association of SH3BP1 and suggested a closer association with adherens than tight junctions (Fig. 4 C). In mouse colon, SH3BP1 and ZO-1 also overlapped, suggesting that the GAP associates with cell junctions in vivo (Fig. 4 D). During de novo junction formation, SH3BP1 was recruited early to forming junctions along with E-cadherin, in agreement with a role in junction assembly (Fig. 4 E).

During the localization experiments, we observed that serum-starved cells had lower levels of junctional SH3BP1 (Fig. S3 A). Addition of EGF led to a rapid increase of the GAP at cell junctions. Conversely, inhibition of EGF receptor signaling with PD153035 led to a reduction of junctional SH3BP1 (Fig. 4 F). Depending on the cellular context, EGF signaling can stimulate cell scattering and junctional remodeling as well as junction stabilization and enhanced barrier function (Van Itallie et al., 1995; Singh and Harris, 2004; Brown et al., 2006; Flores-Benítez et al., 2007; Terakado et al., 2011; Al Moustafa et al., 2012). Hence, SH3BP1 may also support junction formation in response to EGF. A431 cells, in which SH3BP1 regulates calcium-induced junction assembly (Fig. 2), are well suited to address this question as their junctional integrity is EGF dependent (Van Itallie et al., 1995).

In serum-starved A431 cells, both SH3BP1 and ZO-1 were mostly cytosolic. Addition of EGF led to the quick induction of dorsal ruffles to which ZO-1 and other junctional proteins were recruited before appearing at cell junctions along with the formation of a junctional actin belt (Fig. 5 A). SH3BP1 was quickly recruited to dorsal ruffles, indicating that the GAP associates with EGF-induced sites of actin remodeling.

We next tested whether SH3BP1 is also required for EGF-induced actin reorganization and junction formation. Indeed, depletion of the GAP inhibited dorsal ruffle formation, and the cells grew abundant and long filopodia (Fig. 5, B and C). Dorsal recruitment of junctional proteins was consequently also inhibited (Fig. 6 A). Time-lapse microscopy with cells expressing GFP-actin further indicated that depletion of SH3BP1 strongly attenuated EGF-induced actin remodeling. Whereas control siRNA-transfected cells formed extensive and dynamic dorsal ruffles that exhibited the same morphology as in fixed cells, SH3BP1-depleted cells showed little signs of actin dynamics apart from the slow growth of filopodia (Fig. 6 B and Videos 1, 2, 3, and 4).

To determine whether SH3BP1 is generally required for EGF receptor trafficking and/or signaling, we stimulated

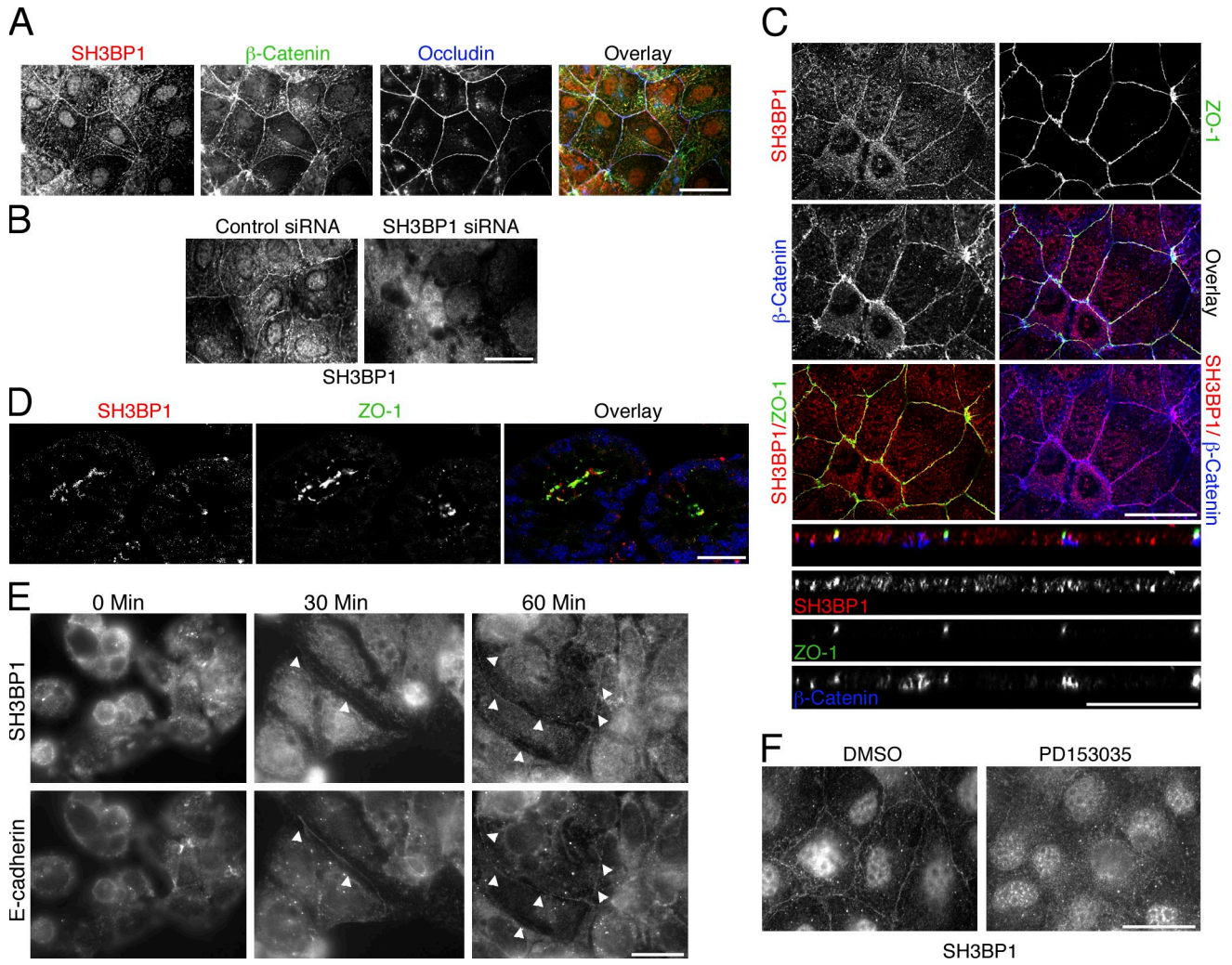

Figure 4. **SH3BP1 associates with the epithelial junctional complex.** (A–C) Caco-2 cells were processed for immunofluorescence with the indicated antibodies and then analyzed by epifluorescence (A and B) or confocal microscopy (C, xy and z sections are shown). For B, cells were transfected with siRNAs as indicated to determine the specificity of the SH3BP1 staining. (D) Frozen sections of mouse colon were stained with antibodies against SH3BP1 and ZO-1. Shown are confocal sections. The overlay also includes a nuclear stain in blue. (E) Junction formation by Caco-2 cells plated in low calcium was stimulated with calcium for the indicated periods to time. The cells were then fixed and stained for SH3BP1 and E-cadherin. Arrowheads mark early E-cadherin– and SH3BP1-positive junctions. (F) Caco-2 cells were stained for SH3BP1 after an incubation with the EGF receptor inhibitor PD153035 or, as a solvent control, DMSO. Bars, 10 µm.

siRNA-transfected cells with fluorescent EGF to monitor receptor internalization. However, the ligand was still internalized in depleted cells, although apparently more slowly (Fig. S3 B). There was no inhibition of extracellular signal–regulated kinase (Erk) activation apparent (Fig. S3 C). Thus, SH3BP1 is not required for EGF receptor signaling per se but for normal actin dynamics and junction assembly.

SH3BP1 spatially restricts Cdc42 signaling

SH3BP1 is a RhoGAP that stimulates GTP hydrolysis by Rac and Cdc42 in vitro and in vivo (Cicchetti et al., 1995; Parrini et al., 2011). To test the importance of this GAP activity, we generated an siRNA-resistant construct carrying a substitution of a conserved arginine residue required for GAP activity (Bos et al., 2007). Whereas the wild-type protein could rescue junction formation in siRNA-transfected cells, the protein lacking a functional GAP domain could not (Fig. 6, C–F). Expression of the GAP mutant in control siRNA-transfected cells already stimulated filopodia, suggesting that it functioned as a dominant-negative mutant (Fig. 6 F). The GAP activity of SH3BP1 is thus important for its role in junction formation.

We next measured the effect of SH3BP1 depletion on the levels of active Cdc42 and Rac in A431 cell extracts. In serum-starved cells, levels of Cdc42 were low and increased upon induction of junction formation by EGF (Fig. 7 A). Depletion of SH3BP1 indeed strongly elevated levels of active Cdc42 during the entire EGF time course, which is in agreement with the observed accumulation of filopodia (Fig. 5). The effect of EGF and SH3BP1 depletion on Rac was limited. A significant small increase in response to depletion of the GAP was only observed after 15 min of EGF stimulation. This indicates that SH3BP1 plays a major role in the regulation of Cdc42 and a more modest role in guiding Rac signaling during junction formation.

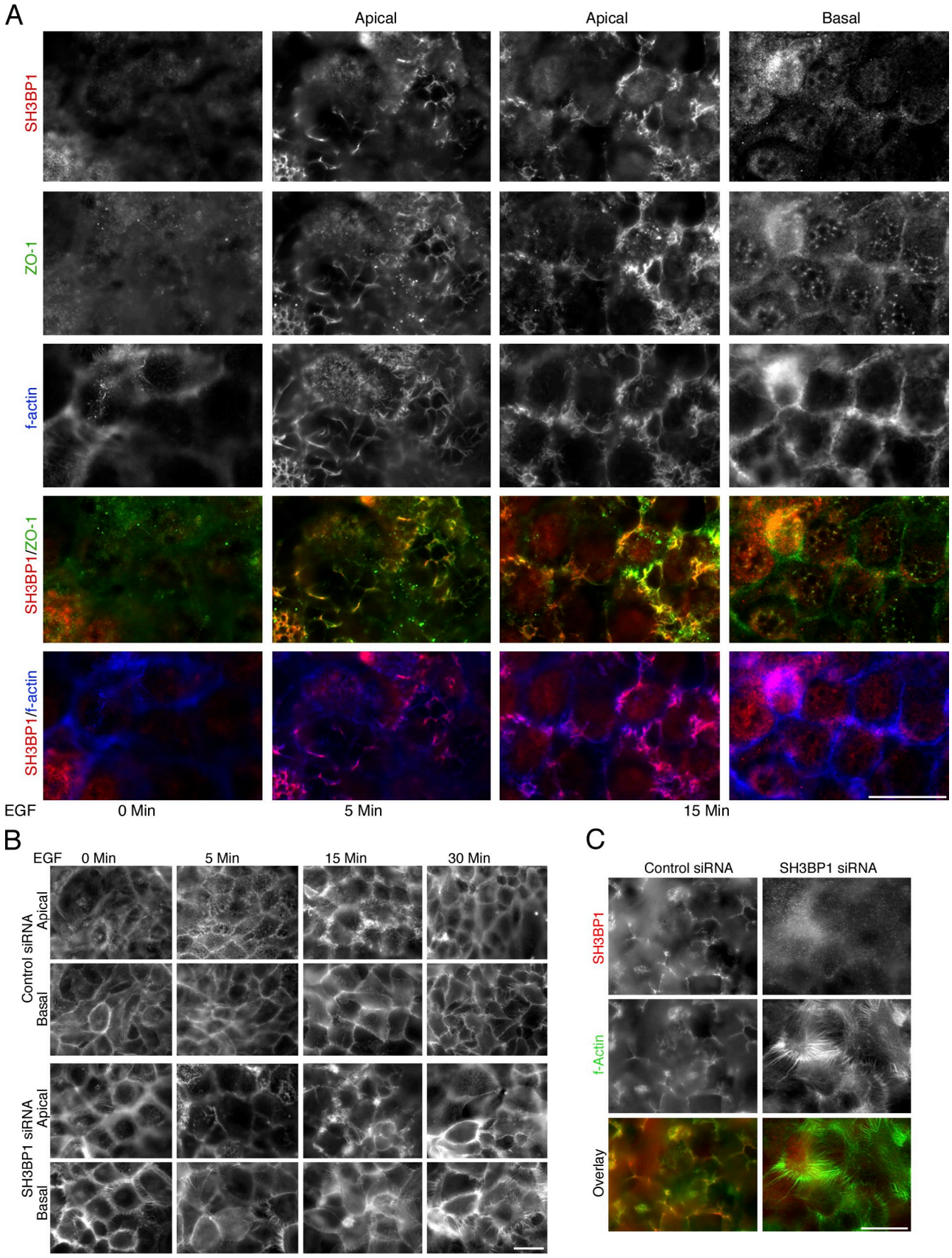

Figure 5. **SH3BP1 regulates EGF-induced dorsal ruffling and junction formation.** (A) A431 cells were serum starved and then stimulated with EGF as indicated. Cells were then fixed, stained, and analyzed by epifluorescence. For the last time point, images from apical and basal focal planes are shown. (B and C) Serum-starved and siRNA-transfected A431 cells were stimulated with EGF and then stained with fluorescent phalloidin and antibodies against SH3BP1. Shown are epifluorescence images. C shows images from the dorsal aspects of the cells. Bars, 10 μm.

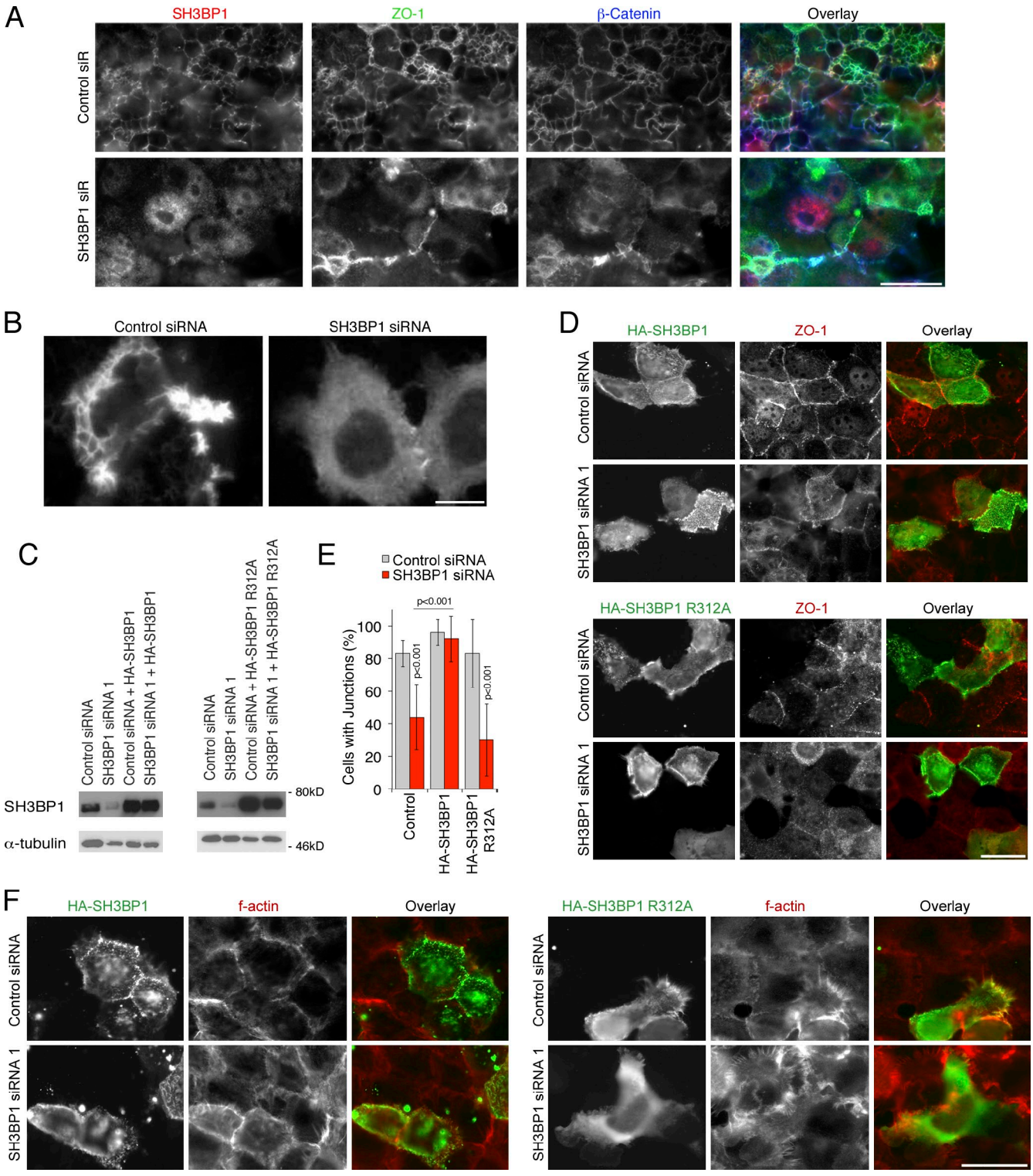

Figure 6. **The GAP activity of SH3BP1 is required for junction formation.** (A) A431 cells were transfected with siRNAs, serum starved, and then stimulated with EGF for 5 min. After fixation, the cells were stained as indicated. Shown are epifluorescence images from the dorsal aspect of the cells. Note that A431 dorsal ruffles are positive for SH3BP1, β-catenin, and ZO-1, which are disrupted upon SH3BP1 depletion. (B) GFP-actin–expressing A431 cells were transfected with siRNAs, serum starved, and then stimulated with EGF. Shown are images of time-lapse recordings taken from the dorsal aspect of the cells. See also Videos 1, 2, 3, and 4. (C–F) A431 cells were transfected with the indicated siRNAs and, after 3 d, with RNAi-resistant cDNAs encoding HA-tagged wild-type or GAP-deficient SH3BP1. The cells were serum depleted, stimulated with EGF, and then analyzed by immunoblotting (C) and immunofluorescence (D–F). E shows a quantification of cells with junctional ZO-1 staining. Shown are means ± 1 SD, representing the cells in at least seven different fields per condition ($n \geq 7$). Note that mutant SH3BP1 has a strong dominant-negative effect on the actin organization. Bars: (A, D, and F) 10 µm; (B) 5 µm.

The enhanced filopodial growth and the increased levels of active Cdc42 suggest that SH3BP1 confines Cdc42 signaling and, thereby, promotes actin remodeling and junction formation. Hence, we used a fluoresecence/Förster resonance energy transfer (FRET)–based biosensor for Cdc42 to test whether depletion of SH3BP1 led to a loss of spatial control of Cdc42 activity (Yoshizaki et al., 2003). In control A431 cells, higher mean FRET activities were measured along the apical surface than along the base of the cells (Fig. 7, B and C). In depleted cells, mean FRET activity was decreased at cell–cell contacts and increased along the base of the cells, correlating with the inhibition of junction formation (Fig. 7 C).

We next used recently developed antibodies specific for the active form of Cdc42 to monitor activation of endogenous GTPases (Fig. S4, A and B, positive controls using Cdc42-specific GEFs; Daubon et al., 2011; Navarro et al., 2011). In serum-starved A431 cells, staining intensity was low, reflecting the low levels of active Cdc42 and indicating that the antibody background was low (Fig. S4 C and Fig. 7 A, Cdc42 levels). Stimulation with EGF resulted in staining of dorsal ruffles within 5 min, in agreement with the previously reported quick and sustained accumulation of active Cdc42 in ruffles (Kurokawa et al., 2004; Kovacs et al., 2006; King et al., 2011). Active Rac1 also increased in response to EGF and was more prominent along the dorsal aspects of the cells; however, it did not accumulate in the large ruffles as active Cdc42 (Fig. S4 D). This is also in agreement with the biosensor experiments by Kurokawa et al. (2004), demonstrating that Rac is transiently activated during ruffle initiation in A431 cells (Kovacs et al., 2006; King et al., 2011). Hence, the results obtained with these antibodies are in agreement with previous work on Rac and Cdc42 activation in the same model system.

In SH3BP1-depleted cells, Cdc42 levels were already higher before adding EGF and then accumulated throughout the cells as well as in filopodia, indicating that the normal spatial organization was lost (Fig. S4 C). Active Rac1 often accumulated in perinuclear cuplike structures in depleted cells, indicating that the spatial organization of Rac1 signaling was also partially disturbed (Fig. S4 D). Deregulated RhoGTPase signaling was also suggested by the increased phosphorylation of cofilin upon SH3BP1 depletion (Fig. S4 E). These observations thus indicate that SH3BP1 regulates the spatial organization of Cdc42 and, in a more modest manner, Rac1 activity.

In Caco-2 cells, the GAP activity of SH3BP1 was also found to be important as the GAP-defective mutant was also found to exert a dominant-negative effect by inducing actin-rich membrane protrusions upon transfection, whereas the wild-type protein did not, even at high expression levels that oversaturated junctional recruitment (Fig. 7 D). Analysis of the spatial distribution of Cdc42 activity supported the importance of SH3BP1 in the regulation of RhoGTPase signaling, as active Cdc42 was enriched apically in control cells but preferentially basal and reduced along cell–cell contacts in depleted cells (Fig. 7, E and F). Staining with the antibodies recognizing active Cdc42 led to the same conclusion, as the staining was enriched at junctions in control cells and dispersed in depleted cells (Fig. 7, G and H; and Fig. S4 F, Cdc42 siRNA control). Lateral or junctional Rac1 staining was not observed. As we did also not obtain clear phenotypes in response to Rac1 depletion or inhibition, Rac1 does not seem to be of importance for junction formation in Caco-2 cells.

As depletion of SH3BP1 led to loss of spatial control of Cdc42 activity, partial depletion of the GTPase might be able to recover the phenotype; hence, we transfected Cdc42-specific siRNAs at suboptimal concentrations either together with nontargeting or SH3BP1-targeting siRNAs. Fig. 8 A shows that 20- and 30-nM Cdc42-specific siRNAs led to a partial depletion of the GTPase; depletion of the GAP was not affected by the cotransfection of different siRNAs. Partial depletion of Cdc42 already interfered with normal junctional assembly but, as expected, not as efficiently as at optimal siRNA concentrations (Fig. 8, B and C). In SH3BP1-depleted cells, partial Cdc42 depletion counteracted the phenotype, and cells formed more regular monolayers with assembled junctions, indicating that Cdc42 is a major functional target of SH3BP1. These data thus indicate that SH3BP1 is an important regulator of epithelial Cdc42 signaling by controlling the spatial organization of the active RhoGTPase, which is supported by the accumulation of SH3BP1 in areas enriched in active Cdc42 during EGF- and calcium-induced junction assembly (Fig. S4, G and H).

SH3BP1 is part of a multimeric, dual activity complex

We next asked whether junctional signaling scaffolds are important for SH3BP1 localization and function. Coimmunoprecipitation revealed that SH3BP1 formed complexes with JACOP/paracingulin, a junctional protein known to affect RhoGTPase signaling, and CD2AP, a scaffolding protein implicated in actin remodeling, in Caco-2 and A431 cells (Fig. 8, A and B; Ohnishi et al., 2004; Bruck et al., 2006; Guillemot et al., 2008; van Duijn et al., 2010; Roldan et al., 2011). JACOP antibodies coprecipitated not only the GAP but also CD2AP, suggesting that the three proteins may exist in a triple complex. Coprecipitation of JACOP with other proteins was not detected, possibly reflecting the low signal obtained in immunoblots of total cell extracts. Coprecipitation of SH3BP1 with several other major components of tight and adherens junctions was not observed (Fig. S5, A and B). Nevertheless, there was coprecipitation of afadin/AF-6, a protein that associates with nectins (Takai et al., 2008), in Caco-2 but not A431 cells, suggesting that SH3BP1 and afadin do not exist in stable complexes in all epithelial cells (Fig. S5 C).

SH3BP1, JACOP, and CD2AP not only form a stable complex but were also found to colocalize at established and forming cell junctions (Fig. 9, C and D) and in EGF-induced dorsal ruffles (Fig. 9 E). Complex formation did not require EGF stimulation (Fig. S5 D), and recruitment of JACOP and CD2AP to cell junctions was, like SH3BP1, attenuated when the EGF receptor was inhibited (Fig. 9 F). Expression levels of the GAP were affected by depletion of JACOP and CD2AP, suggesting that complex formation may be important for stabilization of SH3BP1 (Fig. S5 E). Complex formation was further supported by the enhanced recruitment of CD2AP and SH3BP1 to cell junctions upon overexpression of JACOP (Fig. S5 F).

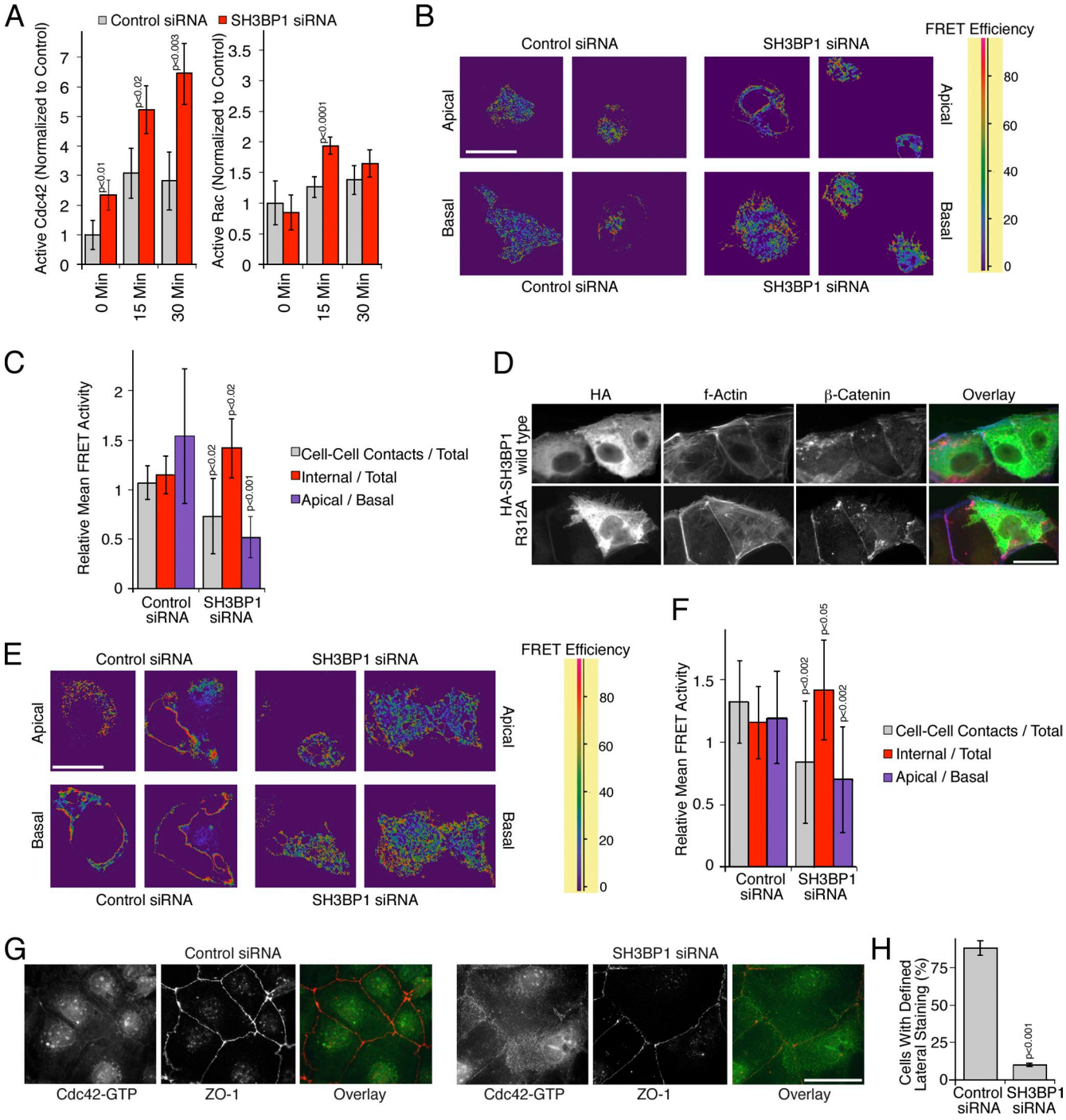

Figure 7. **Spatial regulation of Cdc42 activity by SH3BP1.** (A) Levels of active Cdc42 and Rac1 were measured after serum starvation and stimulation with EGF in total cell extracts after transfection of either control or SH3BP1-targeting siRNAs. Shown are means ± 1 SD (n = 3). (B and C) A431 cells were first transfected with siRNAs and then with a biosensor to measure Cdc42 activity. The cells were then serum starved before stimulating for 10 min with EGF. FRET efficiency was then measured by confocal microscopy. Shown are apical and basal sections. A FRET efficiency scale is shown for the color coding (high FRET efficiency reflects high Cdc42 activity). B shows a quantification of the FRET images, using apical sections to compare internal and cell–cell contact signals and ratios of apical versus basal mean FRET signals. Shown are means of different fields ± 1 SD (n = 11). (D) HA-tagged SH3BP1 constructs encoding the wild-type or a GAP-deficient mutant (R312A) were transfected, and effects on F-actin and β-catenin were analyzed by immunofluorescence and epifluorescence microscopy. (E and F) Caco-2 cells were first transfected with siRNAs and then with the Cdc42 biosensor. FRET efficiency was then measured by confocal microscopy. Shown are apical and basal sections. FRET images were quantified as in C. Shown are means of different fields ± 1 SD (n = 12). (G and H) Caco-2 cells were transfected with siRNAs and then analyzed by immunofluorescence using antibodies against GTP-bound Cdc42 and ZO-1. H shows a quantification of the number of cells with a defined lateral Cdc42 staining as opposed to the diffuse lateral staining observed in SH3BP1-depleted cells. Shown are means ± 1 SD from six different fields (n = 6). Bars, 10 µm.

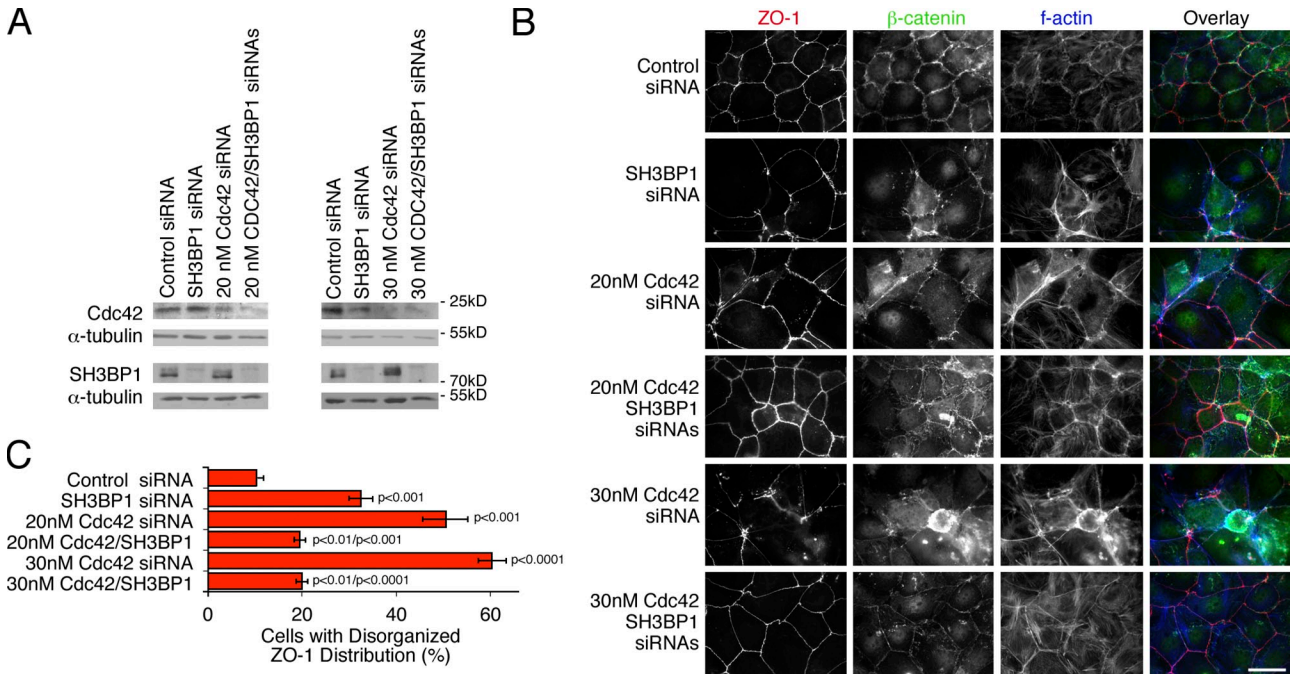

Figure 8. **Cdc42 is a functionally important target of SH3BP1.** Caco-2 cells were transfected with control, SH3BP1-, and Cdc42-specific siRNAs. For Cdc42, two different suboptimal concentrations, 20 and 30 nM, were used. (A and B) Depletion of SH3BP1 and Cdc42 was then analyzed by immunoblotting (A), and the effect on cell morphology and junction assembly was analyzed by immunofluorescence (B). (C) The effect on the ZO-1 distribution was then quantified as in Fig. 1 C. Shown are means ± 1 SD from three independent experiments (n = 3). The indicated p-values for double knockdown data are for comparisons with single SH3BP1 and Cdc42 depletions.

We next used recombinant proteins to map the interacting domains in SH3BP1. Recombinant full-length SH3BP1 as well as a fusion protein containing the C-terminal domain, which includes the SH3-binding domain, pulled down CD2AP (Fig. 9 G). JACOP was only pulled down by the N-terminal domain, suggesting that the recombinant full-length protein might be in a confirmation that does not allow efficient binding. These binding experiments suggest that SH3BP1 might serve as a bridge, linking JACOP to CD2AP. Indeed, coprecipitation of CD2AP with JACOP required SH3BP1, whereas depletion of CD2AP did not affect the coprecipitation efficiency of SH3BP1 with JACOP (Fig. 9 H). The N-terminal domain of SH3BP1 has recently been shown to associate with the exocyst in cells overexpressing the GAP (Parrini et al., 2011); however, we could not detect specific coprecipitation of endogenous proteins.

Similar to SH3BP1, depletion of JACOP or CD2AP also led to an inhibition of actin remodeling and junction formation in both A431 and Caco-2 cells (Fig. 10, A and B; and Fig. S5, G and H). Depletion of JACOP had the strongest effect on the lateral localization of the other components, suggesting that it serves as the primary junctional linker of the complex (Fig. 10 C). Depletion of neither JACOP nor CD2AP led to the same disorganized F-actin appearance, suggesting that disruption of the complex does not stimulate Cdc42. Indeed, depletion of either of the two scaffolding proteins reduced Cdc42 activity (Fig. 10 D), indicating that loss of normal complex formation leads to uncontrolled Cdc42 inactivation.

Previous work showed that CD2AP binds and modulates the activity of CapZα1, a subunit of an F-actin–capping protein that regulates filopodial growth (Mejillano et al., 2004; Bruck et al., 2006). Therefore, we asked whether the SH3BP1–JACOP–paracingulin complex contains two actin-modulating activities: a Rho GAP and an F-actin–capping activity. Indeed, CapZα1 was detected in precipitates of SH3BP1 and the two scaffolding proteins (Fig. 9 B). CapZα1 was recruited to dorsal ruffles along with SH3BP1 in EGF-stimulated A431 cells but remained diffusely distributed in SH3BP1-depleted cells (Fig. 10 E). CapZα1 depletion indeed disrupted formation of a junctional actin belt and induced filopodia (Fig. 10, F and G). Thus, the identified SH3BP1 complex contains two activities that regulate the actin cytoskeleton: a GAP and a capping activity.

Discussion

Here, we have shown that regulation of actin-driven membrane remodeling and junction formation requires an SH3BP1-based complex that modulates the actin cytoskeleton. This complex can regulate two processes: Cdc42 and Rac signaling via the GAP activity of SH3BP1 and actin polymerization via the capping activity of CapZ. It also contains two scaffolding proteins: CD2AP, a protein that is part of the submembrane actin cytoskeleton and binds and regulates CapZ, and JACOP, a junctional protein that mediates subcellular targeting of SH3BP1.

Depletion of SH3BP1 did not only lead to deregulation of Cdc42, but the enhanced and spatially deregulated activity led to the accumulation of large filopodia and a strong reduction of actin dynamics. Hence, maintenance of actin dynamics and morphological transitions rely not simply on Cdc42 activation but require the full GTPase cycle. This is supported by results with dominant-negative and constitutively active Cdc42 that

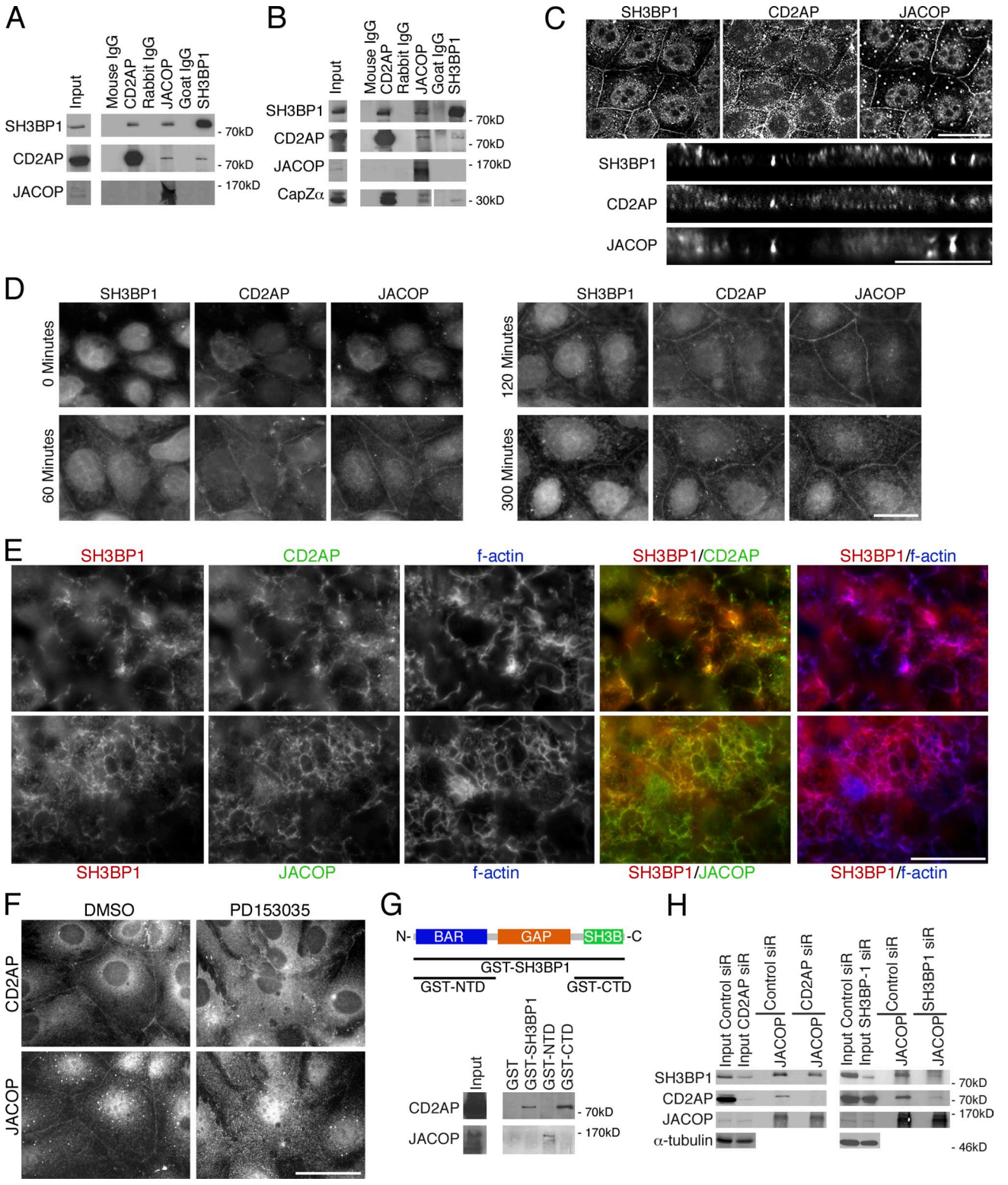

Figure 9. **SH3BP1 forms a complex with CD2AP and the junctional scaffold JACOP.** (A and B) Extracts from Caco-2 (A) and A431 (B) cells were subjected to immunoprecipitation with the indicated antibodies. An IgG control from the same species as each of the specific primary antibodies is shown. The JACOP antibody recognized only a weak band in total cell extracts, and coprecipitation of this protein could not be detected. (C) Caco-2 cells were fixed and processed for immunofluorescence using antibodies against SH3BP1, CD2AP, and JACOP. Shown are confocal xy and z sections. (D) Calcium was added to Caco-2 cells plated in low calcium for the indicated periods to time. The cells were then fixed and stained as indicated. (E) EGF-stimulated A431 cells were fixed and processed as indicated. Shown are epifluorescence images of the dorsal aspect of the cells. Note that CD2AP and JACOP colocalize with SH3BP1 in dorsal ruffles. (F) Caco-2 cells were stained for CD2AP or JACOP after an incubation with the EGF receptor inhibitor PD153035 or, as a solvent control, DMSO. (G) GST fusion proteins conjugated to glutathione beads were incubated with A431 lysate (NTD, N-terminal domain; CTD, C-terminal domain). Pull-down experiments were analyzed by immunoblotting. (H) A431 cells transfected with siRNAs as indicated were lysed, and coprecipitation of CD2AP and SH3BP1 with JACOP was analyzed. Note that depletion of SH3BP1 inhibits coprecipitation of CD2AP. Bars, 10 µm.

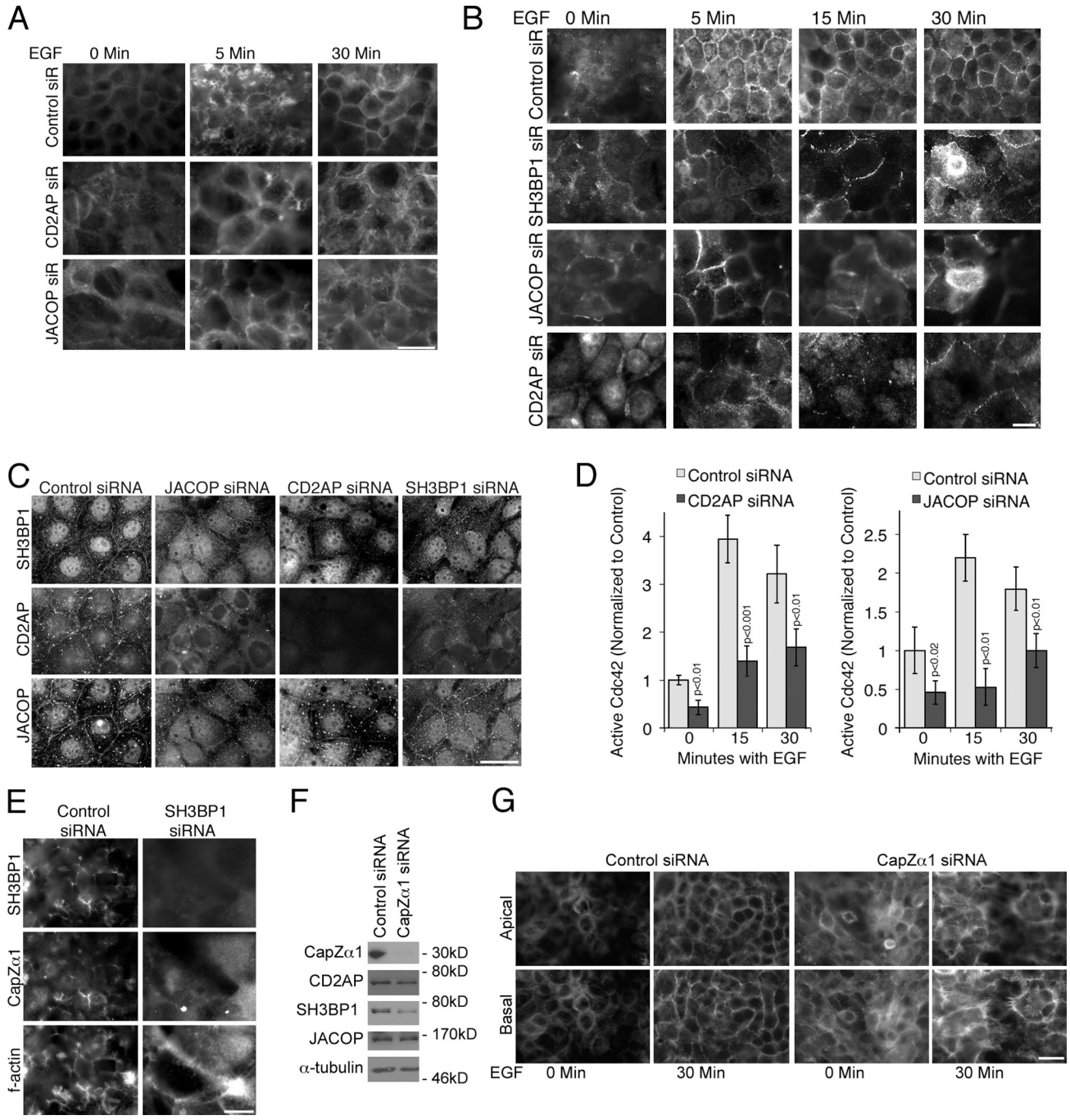

Figure 10. **CD2AP, JACOP, and CapZ are functional components of the SH3BP1 complex.** (A) siRNA-transfected A431 cells were stimulated with EGF and then stained with fluorescent phalloidin. Shown are epifluorescence images of the apical (0 and 5 min) and of the basal (30 min) side of the cells. Note that CD2AP- and JACOP-depleted cells form neither dorsal ruffles nor a cortical actin belt. (B) siRNA-transfected A431 cells were serum starved and then stimulated with EGF for different periods of time. The cells were then fixed and stained for ZO-1. Shown are epifluorescence images taken from the apical part of the cells. Note that depletion of SH3PB1 and its associated proteins prevents the formation of ZO-1–positive ruffles and junctional recruitment. (C) Caco-2 cells transfected with siRNAs targeting SH3BP1, CD2AP, and JACOP were processed for immunofluorescence with antibodies against the three proteins. Shown are epifluorescence images of the junctional region. (D) Levels of active Cdc42 were measured after serum starvation and stimulation with EGF in extracts from cells transfected with either control, CD2AP-, or JACOP-targeting siRNAs. Shown are means ± 1 SD ($n = 4$). (E) A431 cells transfected with control and SH3BP1-targeting siRNAs and, after serum starvation, treated for 5 min with EGF. After fixation, the cells were stained as indicated. Shown are epifluorescence images representing dorsal focal planes. (F) A431 cells transfected with siRNAs targeting CapZα1 were then analyzed by immunoblotting as indicated. (G) A431 cells were siRNA transfected, serum starved, and then stimulated with EGF. The cells were then fixed and stained with fluorescent phalloidin. Shown are epifluorescence images. Note that depletion of CapZα1 leads to induction of filopodia and loss of the junctional actin belt. Bars, 10 μm.

both interfere with junction assembly and epithelial differentiation (Fig. 1 and Fig. S1; Kroschewski et al., 1999; Rojas et al., 2001; Bruewer et al., 2004). Inactivation of Cdc42 is mainly required to prevent excessive activation levels and maintain spatial control, as partial depletion of Cdc42 was sufficient to counteract the effect of SH3BP1 depletion. Similarly, depletion of the GAP corrected the phenotype caused by partial Cdc42 depletion; hence, Cdc42 seems to be the main substrate of SH3BP1 during epithelial junction formation. Although GAPs are counteracting the function of GEFs and, hence, are often seen as inhibiting processes while GEFs promote them, our data show that GAPs, such as SH3BP1, are important to drive progression of complex processes that require sequential morphological steps and cytoskeletal dynamics.

Epithelial junction formation is a complex process that involves sequential steps starting with cell shape changes, initiation of cell–cell contacts, and subsequent maturation to a fully differentiated apical junctional complex consisting of tight and adherens junctions (Vasioukhin et al., 2000; Miyoshi and Takai, 2008; Nelson, 2009). This sequential process requires continuous membrane remodeling driven by the actin cytoskeleton. RhoGTPases play essential roles in these processes, and proper regulation of RhoGTPases is required for successful junction assembly (Braga and Yap, 2005). Our data now show that SH3BP1 is a crucial negative regulator of RhoGTPase and, in particular, Cdc42 signaling, which is required for normal junction assembly and differentiation of epithelial cells from different tissues, and indicate that SH3BP1 is required for the morphological transition from early, immature cell–cell contacts to continuous cell–cell junctions.

Epithelial differentiation seems to rely on different GAPs for Cdc42 that regulate different steps. The Cdc42 GAP Rich1 associates with tight junctions via the Par3–6 complex and regulates apical polarization, not junction assembly (Wells et al., 2006). Thus, epithelial junctions recruit GAPs for Cdc42 with fundamentally different roles: SH3BP1 is recruited early during junction formation and regulates junction assembly, whereas Rich1 regulates polarization once junctions are assembled. Accordingly, we could not detect a defect in junction assembly upon transfection of Rich1-targeting siRNAs in the screen that has led to the identification of SH3BP1 (Table S1).

Although membrane dynamics underlie the initiation of cell contacts in all epithelial models studied, different types of epithelia can make use of different mechanisms of actin-driven processes. Although keratinocytes use filopodia, the kidney epithelial cell line MDCK relies on lamellipodia (Vasioukhin et al., 2000; Ehrlich et al., 2002). As filopodia are induced by Cdc42, whereas lamellipodia require Rac, different GTPases can initiate cell–cell contacts and, as they can both regulate polarity complexes, lead to successful epithelial differentiation (Matter and Balda, 2003b; Nelson, 2009). SH3BP1 was originally identified as a GAP with similar activities toward Cdc42 and Rac1 in vitro (Cicchetti et al., 1995). This was recently confirmed using cell-based biosensor assays (Parrini et al., 2011). The latter paper also demonstrated that SH3BP1 regulates Rac at the front of migrating cells (Parrini et al., 2011). Together with our data, this indicates that SH3BP1 can stimulate GTP hydrolysis by both Rac and Cdc42 in vitro and in vivo and that the activities toward both GTPases are relevant for specific biological processes. Moreover, it could be that SH3BP1 regulates junction formation not only in epithelia that rely on filopodia but also in those that use lamellipodia.

The observations that the GAP activity of SH3BP1 toward Rac and Cdc42 is differentially used in specific cellular processes highlight the importance of the subcellular targeting of the GAP. Although during migration, SH3BP1 is targeted to the front of the cells and regulates Rac, which is active at the leading edge, it is targeted to cell–cell contacts during junction formation and regulates Cdc42, which is active at cell junctions. Similarly, in dorsal ruffles, SH3BP1 strongly affects Cdc42 and, to a lesser extent, Rac1; both GTPases are stimulated during dorsal ruffle formation. Targeting to subcellular sites that are enriched in the active form of either Cdc42 or Rac thus seems to be a major determinant of the GTPase selectivity of the GAP, and its activity seems to prevent the diffusion of active GTPase away from specific sites. Complex formation seems to play a fundamental role for junctional targeting of SH3BP1 and its function, as depletion of JACOP and, to lesser extent, CD2AP resulted in loss of junctional SH3BP1, deregulation of Cdc42, and inhibition of junction formation.

The SH3BP1 complex contains molecules that have different cellular roles. Two of these proteins, JACOP and CD2AP, are scaffolding proteins that are linked to each other by SH3BP1. JACOP, also called paracingulin, is a component of the apical junctional complex and can bind different types of junctional proteins (Ohnishi et al., 2004; Pulimeno et al., 2011). Depletion of JACOP had a strong effect on the junctional recruitment of SH3BP1 and CD2AP and led to a strong reduction in Cdc42 activity, indicating that it is important for recruitment of the complex and the control of the GAP activity of SH3BP1. In MDCK cells, JACOP has been linked to the regulation of Rac and RhoA via two different GEFs (Guillemot et al., 2008); however, this is the first study that links JACOP to the regulation of a GAP and of Cdc42.

CD2AP has been known to be recruited to cell junctions and is a cytoskeletal regulator that has been linked to renal disease and slit diaphragm function, a specialized cell junction formed by podocytes (Dustin et al., 1998; Asanuma and Mundel, 2003; Mustonen et al., 2005; Fukasawa et al., 2009). CD2AP is a regulator of actin dynamics and binds to the barbed-end binding protein CapZ (Mejillano et al., 2004; Bruck et al., 2006). CapZ is also part of the SH3BP1 complex, and its depletion induces filopodia, as has previously been demonstrated by genetic ablation (Mejillano et al., 2004). CD2AP and CapZ thus provide the SH3BP1 complex with a second cellular activity that can guide actin reorganization and membrane remodeling. Given the link of CD2AP to renal disease, it will be important to determine whether and how SH3BP1 and JACOP contribute to normal renal physiology and, if deregulated, play a role in disease development. Because of its association with CapZ, we propose that the SH3BP1 complex represents a dual activity feedback complex required for the coordination of actin-driven morphological processes that is recruited to sites of active membrane remodeling by the scaffolding components JACOP and CD2AP to terminate individual steps, enabling activation of subsequent GTPase-activated processes and junctional maturation.

Materials and methods

RNAi, cDNAs, and transfection

A full-length human SH3BP1 cDNA (NM018957.3) was used to generate HA-tagged constructs that were cloned into a pCDNA4/TO vector (Invitrogen). To generate a mutant allele defective in GAP activity, arginine-312 was replaced by an alanine residue using the mutagenesis kit (QuikChange; Agilent Technologies). For SH3BP1 GST fusion protein constructs, the sequences encoding the indicated domains were cloned into pGEX-4T-3 (GE Healthcare) to generate SH3BP1 full-length, N-terminal domain (containing the BAR [Bin-Amphiphysin-Rvs] domain), and C-terminal domain (containing the SH3-binding domain) fusion proteins. The HA-tagged JACOP cDNA was provided by M. Furuse (Kobe University, Kobe, Japan; Ohnishi et al., 2004), the HA-tagged OPHN1 was provided by P. Billuart (Institut Cochin, Paris, France; Billuart et al., 1998), and the Asef2 cDNA was obtained from D. Billadeau (Mayo Clinic, Rochester, NY; Hamann et al., 2007). The DBL isoform 1 was amplified by PCR and cloned into pcDNA-TO with an N-terminal myc tag (Komai et al., 2002). Sequences targeted in the siRNA screen are provided in Tables S2 and S3. siGENOME and ON-TARGETplus siRNAs were obtained from Thermo Fisher Scientific. For subsequent RNAi experiments, cells were transfected with individual or pools of siGENOME siRNAs for SH3BP1, CGNL1 (JACOP), CD2AP, and CapZα1 as well as nontargeting control siRNAs (Thermo Fisher Scientific). The following sequences were targeted: SH3BP1, 5′-GAUGACAGCCACCCACUUC-3′ and 5′-UGGAGAUUCAGGCCGAUUA-3′; CGNL1, 5′-GCAGGGAGCUCGCAGAAAU-3′, 5′-CGGAGUACCUGAUUGAAUU-3′, 5′-CGAGUAAAGUGCUGGAUGA-3′, and 5′-GGGAGAAAUACGACAGUUA-3′; CD2AP, 5′-GGGCGAACUUAAUGGUAAA-3′ and 5′-GAGCAAAUGAAGUGUAAUA-3′; CapZα1, 5′-GAUGGGCAACAGACUAUUA-3′, 5′-UGAAAGACCAUUAUUCCAA-3′, 5′-CACUAACUGUUUCGAAUGA-3′, and 5′-UCUGUACUGUUUAUGCUAA-3′; and Cdc42, 5′-CGGAAUAUGUACCGACUGU-3′ and 5′- GAUGACCCCUCUACUAUUG-3′. To generate a SH3BP1 cDNA resistant to siRNA2, the sequence 5′-GATGACAGCCACCCACTTC-3′ was changed to 5′-AATGACAGCAACACACTTC-3′. For siRNA transfections, transfection reagent (INTERFERin; Polyplus-transfection, Inc.) was used according to the manufacturer's instructions using a total final siRNA concentration of 20–80 nM (Terry et al., 2011). Samples were collected and processed 3–4 d after transfection. For DNA transfections, 0.5 µg/ml plasmid DNA and transfection reagent (jetPEI; Polyplus-transfection, Inc.) was used according to the manufacturer's instructions. Samples were collected and processed after 24 h.

Antibodies

The following antibodies were used: goat anti-SH3BP1 (Everest Biotech); mouse anti–ZO-1 and mouse antioccludin (Invitrogen); mouse anti-CD2AP, rabbit anti-CGNL1/JACOP, mouse anti-CapZα, rabbit anticingulin, rabbit anti-OPHN1, and rabbit antiflag/OctA (Santa Cruz Biotechnology, Inc.); rabbit antimyc (MBL International); rabbit anti–β-catenin and –α-catenin and mouse anti–β-actin (Sigma-Aldrich); mouse anti–E-cadherin, mouse anti–p120 catenin, mouse antiafadin/AF-6, mouse anticofilin, and mouse anti-Cdc42 (BD); rat anti-HA (Roche); mouse anti–Cdc42-GTP and anti-Rac1GTP (NewEast Biosciences); and mouse anti–p-cofilin, rabbit anti-Erk1/2, and mouse anti–p-Erk (Cell Signaling Technology). The following antibodies were as previously described: rabbit anti-JACOP, rabbit anti–ZO-1, rabbit anti–ZO-2, rabbit anti–ZO-3, mouse anti–α-tubulin, mouse anti-DPPIV, mouse anti–Na^+K^+-ATPase, and mouse and rabbit anti-HA tag epitope (Hauri et al., 1985; Kreis, 1987; Daro et al., 1996; Benais-Pont et al., 2003; Ohnishi et al., 2004; Steed et al., 2009; Terry et al., 2011).

Cell culture, cell lines, 3D morphogenesis, calcium switch, and permeability assays

Human adenocarcinoma colon cells (Caco-2), human epithelial carcinoma cell line (A431), and HCE cells were cultured in DME containing 20% (Caco-2) or 10% (A431 and HCE) heat-inactivated FCS with 100 µg/ml streptomycin and 100 µg/ml penicillin (PAA Laboratories) at 37°C in a 5% CO_2 atmosphere. Cells were cultured and plated for experiments as previously described (Matter et al., 1989; Steed et al., 2009; Terry et al., 2011). EGF was used at a final concentration of 100 ng/ml (PeproTech), and PD153035 (Tocris Bioscience) was used for EGF inhibition. For calcium switch and permeability assays, cells were cultured in 6-well plates for the siRNA transfections and were then replated in low calcium medium containing dialyzed FBS after 24 h (Balda et al., 1996; Terry et al., 2011). Junction formation was then induced by replacing the low calcium with normal medium after another 24 h. Trans-epithelial electrical resistance was measured with a silver/silver-chloride electrode to determine the voltage deflection induced by an alternating current square wave current (±20 µA at 12.5 Hz) using an epithelial voltohmmeter (EVOM; World Precision Instruments) as previously described (Matter and Balda, 2003a). Paracellular permeability was determined using 4-kD FITC-conjugated dextran and 70-kD rhodamine B–conjugated dextran over a time of 3 h (Balda et al., 1996). Fluorescence was then determined with a microplate reader (FLUOstar OPTIMA; BMG Labtech). For 3D morphogenesis, siRNA-transfected Caco-2 cells were plated on top of a layer of growth factor–reduced Matrigel (BD; Jaffe et al., 2008; Terry et al., 2011). In brief, coverslips in 48-well plates were covered with 90 µl Matrigel (9.3 mg/ml) and left to gel to 45 min. 10,000 cells were then plated in 300 µl of low glucose medium containing 2% Matrigel. After 48 h, the medium was replaced with fresh medium containing 2% Matrigel and 0.1 µg/ml cholera toxin. After another 48 h, the medium was carefully replaced with the fresh medium/Matrigel/cholera toxin mix. The samples were then fixed 10 h later.

Immunostaining and microscopy

Fixation with methanol or 3% PFA and permeabilization of cells were performed as previously described (Balda et al., 1996; Matter and Balda, 2003a). For the antibodies against active Cdc42 and Rac1 (NewEast Biosciences), cells were fixed in 3% PFA for 20 min at room temperature or methanol for 5 min at −20°C followed by a 3-min incubation in 0.3% Triton X-100 in blocking buffer (PBS containing 0.5% BSA, 10 mM glycine, and 0.1% sodium azide). The samples were then washed and incubated for 1 h in blocking buffer. After blocking and incubation with primary antibodies, the samples were incubated with the appropriate fluorescent secondary antibodies conjugated to either FITC, Cy3, or Cy5 (Jackson ImmunoResearch Laboratories, Inc.) in blocking buffer. In some experiments, fluorescent phalloidin was used (FITC and TRITC [Sigma-Aldrich]; Alexa Fluor 647 [Molecular Probes]), and Hoechst 33258 was used to label DNA (Invitrogen). Matrigel-grown samples were fixed with PFA and then incubated with blocking buffer containing 0.5% Triton X-100 and 0.1% SDS for 1 h. Antibody incubations were then also performed with the same detergent-containing blocking buffer. For tissue sections, colons were dissected from adult female MF1 mice that had been transcardially perfused with 4% PFA in PBS, in accordance with UK Home Office regulations, embedded in OCT compound (VWR International) and snap frozen. 5-µm sections were then taken using a cryostat. For immunofluorescence staining, the sections were permeabilized with acetone/methanol (33:67) for 10 min at −20°C and then transferred to methanol/DMSO (4:1) for 20 h at 4°C. The samples were then rehydrated with sequential changes of methanol decreasing from 75 to 50 and 25 to 0% in PBS at room temperature for 5–10 min each. Next, the samples were further permeabilized and blocked for 8–10 h at room temperature in a humidified chamber in BSA permeabilization buffer (3% BSA, 1% Triton X-100, 0.5% Na-deoxycholate, 0.2% Na-dodecylsulfate, 150 mM NaCl, and 10 mM Hepes, pH 7.4) containing 5% donkey serum (Sigma-Aldrich). The samples were then incubated with goat anti-SH3BP1 and rabbit anti–ZO-1 for 16 h at room temperature in BSA permeabilization buffer containing 5% donkey serum in a humidified chamber. Afterward, samples were washed with PBS and BSA permeabilization buffer sequentially for 10–15 min in two cycles. Incubation with fluorescently labeled secondary antibodies and Hoechst 33258 in BSA permeabilization buffer was for 6 h at room temperature in BSA permeabilization buffer in a humidified chamber followed by washing with PBS and BSA permeabilization buffer for 10–15 min in two cycles and mounting with ProLong (Life Technologies). All fixed samples were embedded in ProLong Gold antifade reagent. All epifluorescent images of fixed specimens were acquired with a fluorescent microscope (DM IRB; Leica) using a 63×/1.4 NA oil immersion objective fitted with a camera (C4742-95; Hamamatsu Photonics) and simplePCI software (Hamamatsu Photonics). Confocal images were acquired with a confocal laser-scanning microscope (LSM 700; Carl Zeiss) or a confocal microscope (SP2; Leica) using 63×/1.4 NA immersion oil objectives. Immersion oil (518 F; Carl Zeiss) was used for all objectives. Images were acquired at ambient temperature using ZEN 2009 (Carl Zeiss) or LCS (Leica). Images were adjusted for brightness and contrast with Photoshop (Adobe). For FRET experiments, siRNA-transfected cells were plated into eight multiwell chamber slides (ibidi), transfected with pRaichu-Cdc42, and analyzed using a microscope (SP2; 63×/1.4 NA objective, 37°C, in medium with 10 mM Hepes, pH 7.4) and LCS FRET software using the donor recovery after acceptor bleaching protocol (YFP was bleached to 30%; Yoshizaki et al., 2003; Terry et al., 2011). The shown FRET efficiency maps were then generated using the LCS software by calculating the FRET efficiency according to the formal $[(D_{post} - D_{pre})/D_{post}] \times 100$ (D represents donor intensity). For quantification, CFP images were subtracted, and mean FRET intensities were

quantified with ImageJ (National Institutes of Health). For each image, all cell–cell contacts were quantified and as many internal areas; means of all cell–cell contacts and all internal areas in a field then gave one value each per imaged field, and these values were used for the final statistical analysis. Normalizations were performed by dividing mean values obtained for specific fields by the mean values obtained for the entire field imaged. Time-lapse videos of A431 cells expressing an EGFP-actin construct were recorded at 37°C using a microscope (Axiovert 200M; Carl Zeiss) with a 40×/0.6 NA objective and a camera (C4742-95). Videos were acquired with SimplePCI software, recording images every 5 s.

Immunoblotting, immunoprecipitations, GST pull-downs, and RhoGTPase activation assays

Whole-cell lysates were collected after washing twice with PBS before adding SDS-PAGE sample buffer and heating at 70°C for 10 min. Extracts were homogenized with a 23-gauge needle. Samples were processed using standard Western blotting techniques. For immunoprecipitations, Caco-2 cells were extracted at 4°C with 0.5% Triton X-100 in PBS and a cocktail of protease and phosphatase inhibitors (Terry et al., 2011). Extracts were preadsorbed with inactive Sepharose beads for 30 min before addition to antibodies conjugated to protein G–Sepharose beads for 2 h at 4°C. Samples were washed twice with 0.5% Triton X-100 in PBS and once with PBS before adding SDS-PAGE sample buffer. For GST pull-down experiments, cells were extracted with the same buffer at 4°C and preadsorbed with inactive beads as described for immunoprecipitations. Extracts were incubated with glutathione–agarose beads coated with fusion proteins and incubated for 2 h at 4°C before washing as described for immunoprecipitations. For RhoGTPase activation assays, cells were transfected with the appropriate siRNAs in 12-well plates, and after 72–96 h, the protein was harvested and analyzed for levels of active Cdc42 and Rac1 using the respective G-LISA assay kits (Cytoskeleton; Terry et al., 2011).

Statistical analysis

Means and SDs were calculated and provided in the graphs. Respective *n* values are provided in the figure legends. The indicated p-values were obtained with the two-tailed Student's *t* test.

Online supplemental material

Fig. S1 shows identification of GAPs important for junction formation. Fig. S2 shows the regulation of junction formation in Caco-2 cells by SH3BP1. Fig. S3 shows the association of SH3BP1 with cell–cell contacts and EGF receptor signaling. Fig. S4 shows regulation of Cdc42 and Rac signaling by SH3BP1. Fig. S5 shows SH3BP1 and complex formation with CD2AP and JACOP. Video 1 shows actin dynamics at the junctional level in control siRNA-transfected cells. Video 2 shows actin dynamics at the junctional level in SH3BP1 siRNA-transfected cells. Video 3 shows actin dynamics at the dorsal aspect of control siRNA-transfected cells. Video 4 shows actin dynamics at the dorsal aspect of SH3BP1 siRNA-transfected cells. Table S1 shows a summary of the observed phenotypes in the siRNA screen. Tables S2 and S3 list the sequences of the siRNAs used in the primary and secondary screens, respectively. Online supplemental material is available at http://www.jcb.org/cgi/content/full/jcb.201202094/DC1.

We are grateful to Mikio Furuse for kindly providing JACOP antibodies and cDNAs, Pierre Billuart for the OPHN1 cDNA, and Daniel Billadeau for the Asef2 cDNA.

A. Elbediwy received a Biotechnology and Biological Sciences Research Council Studentship. This research was supported by the Wellcome Trust.

Submitted: 16 February 2012
Accepted: 11 July 2012

References

Abouhamed, M., K. Grobe, I.V. San, S. Thelen, U. Honnert, M.S. Balda, K. Matter, and M. Bähler. 2009. Myosin IXa regulates epithelial differentiation and its deficiency results in hydrocephalus. *Mol. Biol. Cell*. 20:5074–5085. http://dx.doi.org/10.1091/mbc.E09-04-0291

Al Moustafa, A.E., A. Achkhar, and A. Yasmeen. 2012. EGF-receptor signaling and epithelial-mesenchymal transition in human carcinomas. *Front Biosci (Schol Ed)*. S4:671–684. http://dx.doi.org/10.2741/S292

Asanuma, K., and P. Mundel. 2003. The role of podocytes in glomerular pathobiology. *Clin. Exp. Nephrol.* 7:255–259. http://dx.doi.org/10.1007/s10157-003-0259-6

Balda, M.S., J.A. Whitney, C. Flores, S. González, M. Cereijido, and K. Matter. 1996. Functional dissociation of paracellular permeability and transepithelial electrical resistance and disruption of the apical-basolateral intramembrane diffusion barrier by expression of a mutant tight junction membrane protein. *J. Cell Biol.* 134:1031–1049. http://dx.doi.org/10.1083/jcb.134.4.1031

Benais-Pont, G., A. Punn, C. Flores-Maldonado, J. Eckert, G. Raposo, T.P. Fleming, M. Cereijido, M.S. Balda, and K. Matter. 2003. Identification of a tight junction–associated guanine nucleotide exchange factor that activates Rho and regulates paracellular permeability. *J. Cell Biol.* 160:729–740. http://dx.doi.org/10.1083/jcb.200211047

Billuart, P., T. Bienvenu, N. Ronce, V. des Portes, M.C. Vinet, R. Zemni, H. Roest Crollius, A. Carrié, F. Fauchereau, M. Cherry, et al. 1998. Oligophrenin-1 encodes a rhoGAP protein involved in X-linked mental retardation. *Nature*. 392:923–926. http://dx.doi.org/10.1038/31940

Bos, J.L., H. Rehmann, and A. Wittinghofer. 2007. GEFs and GAPs: critical elements in the control of small G proteins. *Cell*. 129:865–877. http://dx.doi.org/10.1016/j.cell.2007.05.018

Braga, V.M., and A.S. Yap. 2005. The challenges of abundance: epithelial junctions and small GTPase signalling. *Curr. Opin. Cell Biol.* 17:466–474. http://dx.doi.org/10.1016/j.ceb.2005.08.012

Brown, K.E., A. Baonza, and M. Freeman. 2006. Epithelial cell adhesion in the developing *Drosophila* retina is regulated by Atonal and the EGF receptor pathway. *Dev. Biol.* 300:710–721. http://dx.doi.org/10.1016/j.ydbio.2006.08.003

Bruck, S., T.B. Huber, R.J. Ingham, K. Kim, H. Niederstrasser, P.M. Allen, T. Pawson, J.A. Cooper, and A.S. Shaw. 2006. Identification of a novel inhibitory actin-capping protein binding motif in CD2-associated protein. *J. Biol. Chem.* 281:19196–19203. http://dx.doi.org/10.1074/jbc.M600166200

Bruewer, M., A.M. Hopkins, M.E. Hobert, A. Nusrat, and J.L. Madara. 2004. RhoA, Rac1, and Cdc42 exert distinct effects on epithelial barrier via selective structural and biochemical modulation of junctional proteins and F-actin. *Am. J. Physiol. Cell Physiol.* 287:C327–C335. http://dx.doi.org/10.1152/ajpcell.00087.2004

Chhabra, E.S., and H.N. Higgs. 2007. The many faces of actin: matching assembly factors with cellular structures. *Nat. Cell Biol.* 9:1110–1121. http://dx.doi.org/10.1038/ncb1007-1110

Cicchetti, P., A.J. Ridley, Y. Zheng, R.A. Cerione, and D. Baltimore. 1995. 3BP-1, an SH3 domain binding protein, has GAP activity for Rac and inhibits growth factor-induced membrane ruffling in fibroblasts. *EMBO J.* 14:3127–3135.

Daro, E., P. van der Sluijs, T. Galli, and I. Mellman. 1996. Rab4 and cellubrevin define different early endosome populations on the pathway of transferrin receptor recycling. *Proc. Natl. Acad. Sci. USA*. 93:9559–9564. http://dx.doi.org/10.1073/pnas.93.18.9559

Daubon, T., R. Buccione, and E. Génot. 2011. The Aarskog-Scott syndrome protein Fgd1 regulates podosome formation and extracellular matrix remodeling in transforming growth factor β-stimulated aortic endothelial cells. *Mol. Cell. Biol.* 31:4430–4441. http://dx.doi.org/10.1128/MCB.05474-11

Dustin, M.L., M.W. Olszowy, A.D. Holdorf, J. Li, S. Bromley, N. Desai, P. Widder, F. Rosenberger, P.A. van der Merwe, P.M. Allen, and A.S. Shaw. 1998. A novel adaptor protein orchestrates receptor patterning and cytoskeletal polarity in T-cell contacts. *Cell*. 94:667–677. http://dx.doi.org/10.1016/S0092-8674(00)81608-6

Ehrlich, J.S., M.D. Hansen, and W.J. Nelson. 2002. Spatio-temporal regulation of Rac1 localization and lamellipodia dynamics during epithelial cell-cell adhesion. *Dev. Cell*. 3:259–270. http://dx.doi.org/10.1016/S1534-5807(02)00216-2

Flores-Benítez, D., A. Ruiz-Cabrera, C. Flores-Maldonado, L. Shoshani, M. Cereijido, and R.G. Contreras. 2007. Control of tight junctional sealing: role of epidermal growth factor. *Am. J. Physiol. Renal Physiol.* 292:F828–F836. http://dx.doi.org/10.1152/ajprenal.00369.2006

Fukasawa, H., S. Bornheimer, K. Kudlicka, and M.G. Farquhar. 2009. Slit diaphragms contain tight junction proteins. *J. Am. Soc. Nephrol.* 20:1491–1503. http://dx.doi.org/10.1681/ASN.2008101117

Guillemot, L., S. Paschoud, L. Jond, A. Foglia, and S. Citi. 2008. Paracingulin regulates the activity of Rac1 and RhoA GTPases by recruiting Tiam1 and GEF-H1 to epithelial junctions. *Mol. Biol. Cell*. 19:4442–4453. http://dx.doi.org/10.1091/mbc.E08-06-0558

Hamann, M.J., C.M. Lubking, D.N. Luchini, and D.D. Billadeau. 2007. Asef2 functions as a Cdc42 exchange factor and is stimulated by the release of an autoinhibitory module from a concealed C-terminal activation element. *Mol. Cell. Biol.* 27:1380–1393. http://dx.doi.org/10.1128/MCB.01608-06

Hauri, H.-P., E.E. Sterchi, D. Bienz, J.A.M. Fransen, and A. Marxer. 1985. Expression and intracellular transport of microvillus membrane hydrolases in human intestinal epithelial cells. *J. Cell Biol.* 101:838–851. http://dx.doi.org/10.1083/jcb.101.3.838

Iden, S., and J.G. Collard. 2008. Crosstalk between small GTPases and polarity proteins in cell polarization. *Nat. Rev. Mol. Cell Biol.* 9:846–859. http://dx.doi.org/10.1038/nrm2521

Jaffe, A.B., and A. Hall. 2005. Rho GTPases: biochemistry and biology. *Annu. Rev. Cell Dev. Biol.* 21:247–269. http://dx.doi.org/10.1146/annurev.cellbio.21.020604.150721

Jaffe, A.B., N. Kaji, J. Durgan, and A. Hall. 2008. Cdc42 controls spindle orientation to position the apical surface during epithelial morphogenesis. *J. Cell Biol.* 183:625–633. http://dx.doi.org/10.1083/jcb.200807121

Khelfaoui, M., A. Pavlowsky, A.D. Powell, P. Valnegri, K.W. Cheong, Y. Blandin, M. Passafaro, J.G. Jefferys, J. Chelly, and P. Billuart. 2009. Inhibition of RhoA pathway rescues the endocytosis defects in Oligophrenin1 mouse model of mental retardation. *Hum. Mol. Genet.* 18:2575–2583. http://dx.doi.org/10.1093/hmg/ddp189

King, S.J., D.C. Worth, T.M. Scales, J. Monypenny, G.E. Jones, and M. Parsons. 2011. β1 integrins regulate fibroblast chemotaxis through control of N-WASP stability. *EMBO J.* 30:1705–1718. http://dx.doi.org/10.1038/emboj.2011.82

Komai, K., R. Okayama, M. Kitagawa, H. Yagi, K. Chihara, and S. Shiozawa. 2002. Alternative splicing variants of the human DBL (MCF-2) proto-oncogene. *Biochem. Biophys. Res. Commun.* 299:455–458. http://dx.doi.org/10.1016/S0006-291X(02)02645-1

Kovacs, E.M., R.S. Makar, and F.B. Gertler. 2006. Tuba stimulates intracellular N-WASP-dependent actin assembly. *J. Cell Sci.* 119:2715–2726. http://dx.doi.org/10.1242/jcs.03005

Kreis, T.E. 1987. Microtubules containing detyrosinated tubulin are less dynamic. *EMBO J.* 6:2597–2606.

Kroschewski, R., A. Hall, and I. Mellman. 1999. Cdc42 controls secretory and endocytic transport to the basolateral plasma membrane of MDCK cells. *Nat. Cell Biol.* 1:8–13. http://dx.doi.org/10.1038/8977

Kurokawa, K., R.E. Itoh, H. Yoshizaki, Y.O. Nakamura, and M. Matsuda. 2004. Coactivation of Rac1 and Cdc42 at lamellipodia and membrane ruffles induced by epidermal growth factor. *Mol. Biol. Cell.* 15:1003–1010. http://dx.doi.org/10.1091/mbc.E03-08-0609

Matter, K., and M.S. Balda. 2003a. Functional analysis of tight junctions. *Methods.* 30:228–234. http://dx.doi.org/10.1016/S1046-2023(03)00029-X

Matter, K., and M.S. Balda. 2003b. Signalling to and from tight junctions. *Nat. Rev. Mol. Cell Biol.* 4:225–236. http://dx.doi.org/10.1038/nrm1055

Matter, K., W. McDowell, R.T. Schwartz, and H.P. Hauri. 1989. Asynchronous transport to the cell surface of intestinal brush border hydrolases is not due to differential trimming of N-linked oligosaccharides. *J. Biol. Chem.* 264:13131–13139.

Mejillano, M.R., S. Kojima, D.A. Applewhite, F.B. Gertler, T.M. Svitkina, and G.G. Borisy. 2004. Lamellipodial versus filopodial mode of the actin nanomachinery: pivotal role of the filament barbed end. *Cell.* 118:363–373. http://dx.doi.org/10.1016/j.cell.2004.07.019

Miyoshi, J., and Y. Takai. 2008. Structural and functional associations of apical junctions with cytoskeleton. *Biochim. Biophys. Acta.* 1778:670–691. http://dx.doi.org/10.1016/j.bbamem.2007.12.014

Mustonen, H., A. Lepistö, S. Lehtonen, E. Lehtonen, P. Puolakkainen, and E. Kivilaakso. 2005. CD2AP contributes to cell migration and adhesion in cultured gastric epithelium. *Biochem. Biophys. Res. Commun.* 332:426–432. http://dx.doi.org/10.1016/j.bbrc.2005.04.140

Navarro, A., R.E. Perez, M.H. Rezaiekhaligh, S.M. Mabry, and I.I. Ekekezie. 2011. Polarized migration of lymphatic endothelial cells is critically dependent on podoplanin regulation of Cdc42. *Am. J. Physiol. Lung Cell. Mol. Physiol.* 300:L32–L42. http://dx.doi.org/10.1152/ajplung.00171.2010

Nelson, W.J. 2009. Remodeling epithelial cell organization: transitions between front-rear and apical-basal polarity. *Cold Spring Harb. Perspect. Biol.* 1:a000513. http://dx.doi.org/10.1101/cshperspect.a000513

Ohnishi, H., T. Nakahara, K. Furuse, H. Sasaki, S. Tsukita, and M. Furuse. 2004. JACOP, a novel plaque protein localizing at the apical junctional complex with sequence similarity to cingulin. *J. Biol. Chem.* 279:46014–46022. http://dx.doi.org/10.1074/jbc.M402616200

Omelchenko, T., and A. Hall. 2012. Myosin-IXA regulates collective epithelial cell migration by targeting RhoGAP activity to cell-cell junctions. *Curr. Biol.* 22:278–288. http://dx.doi.org/10.1016/j.cub.2012.01.014

Parrini, M.C., A. Sadou-Dubourgnoux, K. Aoki, K. Kunida, M. Biondini, A. Hatzoglou, P. Poullet, E. Formstecher, C. Yeaman, M. Matsuda, et al. 2011. SH3BP1, an exocyst-associated RhoGAP, inactivates Rac1 at the front to drive cell motility. *Mol. Cell.* 42:650–661. http://dx.doi.org/10.1016/j.molcel.2011.03.032

Pulimeno, P., S. Paschoud, and S. Citi. 2011. A role for ZO-1 and PLEKHA7 in recruiting paracingulin to tight and adherens junctions of epithelial cells. *J. Biol. Chem.* 286:16743–16750. http://dx.doi.org/10.1074/jbc.M111.230862

Redd, M.J., L. Cooper, W. Wood, B. Stramer, and P. Martin. 2004. Wound healing and inflammation: embryos reveal the way to perfect repair. *Philos. Trans. R. Soc. Lond. B Biol. Sci.* 359:777–784. http://dx.doi.org/10.1098/rstb.2004.1466

Ridley, A.J. 2006. Rho GTPases and actin dynamics in membrane protrusions and vesicle trafficking. *Trends Cell Biol.* 16:522–529. http://dx.doi.org/10.1016/j.tcb.2006.08.006

Rojas, R., W.G. Ruiz, S.M. Leung, T.S. Jou, and G. Apodaca. 2001. Cdc42-dependent modulation of tight junctions and membrane protein traffic in polarized Madin-Darby canine kidney cells. *Mol. Biol. Cell.* 12:2257–2274.

Roldan, J.L., M. Blackledge, N.A. van Nuland, and A.I. Azuaga. 2011. Solution structure, dynamics and thermodynamics of the three SH3 domains of CD2AP. *J. Biomol. NMR.* 50:103–117. http://dx.doi.org/10.1007/s10858-011-9505-5

Singh, A.B., and R.C. Harris. 2004. Epidermal growth factor receptor activation differentially regulates claudin expression and enhances transepithelial resistance in Madin-Darby canine kidney cells. *J. Biol. Chem.* 279:3543–3552. http://dx.doi.org/10.1074/jbc.M308682200

Steed, E., N.T. Rodrigues, M.S. Balda, and K. Matter. 2009. Identification of MarvelD3 as a tight junction-associated transmembrane protein of the occludin family. *BMC Cell Biol.* 10:95. http://dx.doi.org/10.1186/1471-2121-10-95

Takai, Y., W. Ikeda, H. Ogita, and Y. Rikitake. 2008. The immunoglobulin-like cell adhesion molecule nectin and its associated protein afadin. *Annu. Rev. Cell Dev. Biol.* 24:309–342. http://dx.doi.org/10.1146/annurev.cellbio.24.110707.175339

Terakado, M., Y. Gon, A. Sekiyama, I. Takeshita, Y. Kozu, K. Matsumoto, N. Takahashi, and S. Hashimoto. 2011. The Rac1/JNK pathway is critical for EGFR-dependent barrier formation in human airway epithelial cells. *Am. J. Physiol. Lung Cell. Mol. Physiol.* 300:L56–L63. http://dx.doi.org/10.1152/ajplung.00159.2010

Terry, S.J., C. Zihni, A. Elbediwy, E. Vitiello, I.V. Leefa Chong San, M.S. Balda, and K. Matter. 2011. Spatially restricted activation of RhoA signalling at epithelial junctions by p114RhoGEF drives junction formation and morphogenesis. *Nat. Cell Biol.* 13:159–166. http://dx.doi.org/10.1038/ncb2156

van Duijn, T.J., E.C. Anthony, P.J. Hensbergen, A.M. Deelder, and P.L. Hordijk. 2010. Rac1 recruits the adapter protein CMS/CD2AP to cell-cell contacts. *J. Biol. Chem.* 285:20137–20146. http://dx.doi.org/10.1074/jbc.M109.099481

Van Itallie, C.M., M.S. Balda, and J.M. Anderson. 1995. Epidermal growth factor induces tyrosine phosphorylation and reorganization of the tight junction protein ZO-1 in A431 cells. *J. Cell Sci.* 108:1735–1742.

Vasioukhin, V., C. Bauer, M. Yin, and E. Fuchs. 2000. Directed actin polymerization is the driving force for epithelial cell-cell adhesion. *Cell.* 100:209–219. http://dx.doi.org/10.1016/S0092-8674(00)81559-7

Wells, C.D., J.P. Fawcett, A. Traweger, Y. Yamanaka, M. Goudreault, K. Elder, S. Kulkarni, G. Gish, C. Virag, C. Lim, et al. 2006. A Rich1/Amot complex regulates the Cdc42 GTPase and apical-polarity proteins in epithelial cells. *Cell.* 125:535–548. http://dx.doi.org/10.1016/j.cell.2006.02.045

Yoshizaki, H., Y. Ohba, K. Kurokawa, R.E. Itoh, T. Nakamura, N. Mochizuki, K. Nagashima, and M. Matsuda. 2003. Activity of Rho-family GTPases during cell division as visualized with FRET-based probes. *J. Cell Biol.* 162:223–232. http://dx.doi.org/10.1083/jcb.200212049